Attention is drawn to the fact that the copyright of this thesis rests with its author.

This copy of the thesis has been supplied on condition that anyone who consults it is understood to recognise that its copyright rests with its author and that no quotation from the thesis and no information derived from it may be published without the author's prior written consent.

D12778 175
Koschmieder, H.
pp 114

EXCITATION OF ATOMS BY ELECTRON IMPACT NEAR THRESHOLD

by

Herbert Koschmieder

Thesis submitted to the
University of Stirling
for the degree of
Doctor of Philosophy

University of Stirling
Stirling
1974

ABSTRACT

A crossed beam apparatus for the measurement of excitation cross sections by electron impact for atomic hydrogen and the rare gases has been built which includes a high intensity long-channel beam source producing beam densities of the order of 10^{11} atoms/cm^3. The atom beam was crossed by an energy selected electron beam with a full width at half maximum of about 100 meV, produced by a cylindrical electron monochromator.

The excitation function of the 2s state in atomic hydrogen and of the $4p^5$ 5s states in krypton and the $5p^5$ 6s states in xenon has been measured.

In the case of atomic hydrogen, the metastable 2s-atoms were detected by observing the Lyman-α photons emitted as a result of quenching in an electric field. Absolute values for the cross section were obtained by normalizing to the close-coupling calculations of Burke et al. The resonance structure at 11.7 eV, which is a superposition of the ^1S and ^3P resonances predicted by Burke at al, has been detected.

The excitation function of the first excited levels of krypton and xenon with the configuration $4p^5$ 5s and $5p^5$ 6s respectively has been measured by observing the ultraviolet photons from the decay of these states. In the threshold region, the excitation functions are found to be dominated by resonances. Comparison is made with other experimental results.

ACKNOWLEDGEMENTS

I wish to thank Professor H. Kleinpoppen for supporting this work and for his encouragement and interest in its progress.

My particular thanks go to Mr. V. Raible, with whom it was a pleasure to collaborate in this experiment and whose assistance in overcoming the difficulties associated with this experiment was invaluable.

My thanks go also to the other members of the Physics Department for their assistance and for useful discussions and comments, in particular to Dr. A. J. Duncan who read the manuscript.

I also wish to thank the technical staff of the Physics Department and of Shared Technical Services of the University of Stirling, in particular Mr. R. R. Harrison and Mr. J. Stewart who helped in the design and construction of the apparatus; Mr. G. O'Neill and Mr. W. D. Stirling, who built some of the critical components of the apparatus.

I would also like to thank Dr. A. Oed of the University of Tübingen (Germany) for useful discussions.

TABLE OF CONTENTS

Abstract

Acknowledgements

1. Introduction

2. Previous Experiments

3. Statement of Problem

3.1 Definition of the Cross Section

3.2 Crossed Beam Technique

3.3 Basis of Experiment

3.4 Experimental Approach

4. Theory

4.1 Introduction

4.2 Basic Concepts and Definitions

4.3 Theory of Electron-Hydrogen Scattering

4.4 Resonances

4.4.1 Results for Atomic Hydrogen

4.4.2 Results for the Heavy Rare Gases

5. The Apparatus

5.1 The Vacuum System

5.1.1 General Description

5.1.2 The Oven Chamber

5.1.3 The Excitation Chamber

5.1.4 The Gas Handling System

5.2 The Atom Beam Source

5.2.1 Beam Formation

5.2.2 Mechanical Design of the Oven

5.2.3 Operating Characteristics

5.3 The Electron Monochromator

5.3.1 Introduction

5.3.2 Mechanical Design

5.3.3 Electrical Supplies

5.3.4 Operating Characteristics

5.4 The Quenching Field and the Detector

5.4.1 Introduction

5.4.2 The Geometry and Mechanical Construction

5.4.3 The Photon Detector

5.5. Modifications for the Rare Gases

6. Electronics and Data Acquisition

6.1 General Description

6.2 Multichannel Analyser and Energy Scanning

7. Measurement of the Excitation Cross Section

7.1 Excitation of the 2s-state in H

7.1.1 Alignment of the Apparatus and Signal Tests

7.1.2 Cross Section Measurements

7.1.3 Evaluation of Data

7.1.4 Results for the H(2s) Excitation Cross Section

7.2 Excitation of the $4p^5 5s$ states in Krypton and the $5p^5 6s$-states in Xenon

7.2.1 Results for Krypton and Xenon

7.3 Conclusions and Suggestions for Further Work

1. Introduction

In the early 1960's the interest of collision physicists in the electron-atom scattering problem shifted from the high energy region to low energies, in the case of elastic collisions to the region below the first inelastic threshold and in the case of inelastic collisions to the threshold region.

There were two reasons for this, one theoretical and one experimental.

With the introduction of high speed computers, it became possible to apply sophisticated theoretical methods, such as the close coupling approximation, to both elastic and inelastic scattering at low energies. These calculations predicted resonance structure in the elastic scattering cross section of electrons from atomic hydrogen. (Burke and Schey 1962).

The close coupling method, which is based on the expansion of the total wave function of the system electron-atom, in terms of eigenfunctions of the target atom, was then applied to the excitation of the hydrogen 2s and 2p states and the result was a series of narrow resonances in the cross section below the n=3 threshold. (Burke, Ormonde and Whitaker 1967). A narrow resonance just above the n=2 threshold was also predicted (Taylor and Burke 1967).

The scattering of electrons from atomic hydrogen has always been of special interest, since from the theoretical point of view it is the fundamental scattering problem. The theoretical approaches used to solve this problem have been reviewed by Moiseiwitsch and Smith (1968).

The resonances can be explained by postulating the formation of compound states of the H^--ion which decay with a lifetime of the order of 10^{-13} sec by the emission of the electron, according to the scheme $e + H(1s) \rightarrow (H^-)^* \rightarrow e + H(1s)$.

The formation of compound states of projectile + target nucleus is a well known process in nuclear physics, and is manifested in the Breit-Wigner resonances in processes such as $B^{10} + He^4 \rightarrow (N^{14})^* \rightarrow p + C^{13}$. The formation of the compound nucleus $(N^{14})^*$ is a resonant process, which occurs whenever the energy of the α-particle coincides with the excitation energy of the compound state. Usually, there are several competing decay processes for the compound nucleus and similar results can be expected for the compound state $(H^-)^*$, making inelastic processes such as $e + H(1s) \rightarrow (H^-)^* \rightarrow e + H(2s)$ possible, provided the energy of the electrons is high enough to excite the higher lying compound states.

On the experimental side, it became possible to look at the fine structure in the cross section at low energies using the newly developed electron monochromators for low energy electrons which reduced the energy spread of electron beams to less than 100 meV. Typical energy widths of resonances are 10-40 meV.

Resonance structure in the elastic scattering of electrons from helium at 19.30 eV (Schulz 1963) and from atomic hydrogen at 9.7 eV (Schulz 1964) was soon discovered. The resonance in helium has since been investigated in great detail and its energy position accurately determined,

and it is often used for energy calibration purposes. In the inelastic scattering channel in helium, resonances were also detected by Chamberlain and Heideman (1965). They investigated inelastic scattering at zero angle for the n=2 levels in He and showed that the threshold excitation is dominated by resonances.

One of the reasons why the resonances were first detected in helium is that the rare gases are monoatomic at room temperatures and a static gas target of high density can be used.

Experimentally, atomic hydrogen presents great difficulties, since the gas is molecular at room temperature. The molecules must be dissociated and the experiment must be performed with crossed electron and atom beams with densities much smaller than those of static gas targets. In a high resolution experiment, when using monochromatic electron beams with low intensity, counting of single photons or electrons becomes necessary.

In the last few years, interest has arisen in the excitation of the heavy rare gases, which have been hitherto neglected, compared with helium. In common with hydrogen and helium, near-threshold excitation is expected to be dominated by resonance structure. The resonances in elastic scattering are already known. The situation differs from hydrogen in as far as there are very few theoretical calculations with which experiments can be compared.

The aim of the present experiment was to build an atomic beam apparatus which would allow measurement of the

excitation cross sections and elastic scattering cross sections of atoms. The other experiments carried out on this apparatus are described in the thesis by V. Raible (1974).

The first atom to be studied was atomic hydrogen, the aim being to investigate the threshold behaviour of the excitation of the 2s state with high energy resolution in order to detect the resonances predicted by theory. The excitation cross section of the $4p^5 5s$ states in krypton and the $5p^5 6s$ states in xenon were also studied in order to verify the existence of resonance structure in the threshold region.

In Chapter 2, previous experiments are reviewed; in Chapter 3, the experimental problem is discussed; and in Chapter 4 the relevant theory is presented.

The details of the apparatus are described in Chapter 5 and 6, and all the results and conclusions are presented in Chapter 7.

2. Previous Experiments

Prior to 1960, all scattering experiments were made using electron beams with a thermal energy width of 300 - 500 meV. Experimentalists therefore put great effort into the construction of electron monochromators with improved energy resolution, and among these the cylindrical 127° type (Marmet and Kerwin 1960) and the hemispherical type (Kuyatt and Simpson 1967) have found the widest application in scattering experiments.

The first high resolution measurement of an excitation

cross section in atomic hydrogen was made by McGowan, Williams and Curley (1969) who confirmed the existence of resonance structure for the 1s-2p excitation cross section, using a cylindrical electron monochromator with an energy width of 70 meV. There is, however, no high resolution measurement of the 1s-2s excitation cross section.

Lamb and Retherford (1951) pioneered the crossed beam technique in atomic hydrogen using a thermal dissociator in their classic series of papers on the Lamb shift and also made the first measurement of the 1s-2s excitation function.

The subsequent experiments using crossed beams studied this excitation process in more detail. (Lichten and Schultz 1959; Stebbings, Fite, Hummer and Brackmann 1960; Hils, Kleinpoppen and Koschmieder 1966; Kauppila, Ott and Fite 1970; Cox and Smith 1971; Oed 1971). Most of these experiments measured the excitation up to energies of a few hundred eV in order to obtain absolute values for the cross sections by normalizing to the Born approximation. An absolute measurement would involve measuring the target beam density and this has not yet been attempted.

Of the above experiments, those of Lichten and Schultz, Hils et al, and Oed investigated the cross section in the threshold region in detail. In the first two, the thermal energy spread was too large for the resonance structure to be resolved. Oed, however, reduced his energy spread somewhat by reducing the cathode temperature of his electron gun and by virtue of a very high signal-to-noise ratio was able to show the existence of structure. The aim of the present experiment was to further improve the energy

resolution by using an electron monochromator.

In the case of the heavy rare gases, all the experiments on excitation cross sections have been carried out during the last few years. In common with hydrogen and helium, the formation of compound states of the negative ion leading to resonances is expected to occur, and resonances in elastic scattering have been known since 1965. (Kuyatt, Simpson and Mielczarek 1965). It was therefore decided to investigate the threshold region of the excitation cross section of the first excited states in krypton and xenon in order to detect resonances in other channels than previously studied and compare these measurements with related experiments.

Very extensive studies of the excitation of metastable states (Pichanick and Simpson 1968) and resonances in transmission (Sanche and Schulz 1972) are available for all the rare gases and they show resonances above the first excitation threshold.

In the particular case of krypton, the excitation of the lowest excited states has very recently been investigated by detecting the inelastically scattered electrons (Swanson, Cooper and Kuyatt 1973) but no optical measurement is available. Measurements of the corresponding excitation function in xenon have been reported recently. (Elston, Lawton and Pichanick 1973).

3. Statement of Problem

3.1 Definition of the Cross Section

Consider a parallel beam of electrons moving in the z-direction, with a flux density j. The number N of

electrons scattered per second by a fixed scattering centre into a solid angle $d\omega$ in the direction (θ, ϕ) can be written as,

$$N = d\omega \; j \; \sigma \; (\theta, \phi) \quad . \qquad (3.1.1)$$

The quantity $\sigma \; (\theta, \phi)$, which has the dimension of an area, is called the differential cross section for scattering in the direction (θ, ϕ).

The total number of electrons scattered into all directions is given by $Z = j \; Q$ where Q, the total cross section, is given by,

$$Q = \int_0^{\pi} \int_0^{2\pi} \sigma \; (\theta, \phi) \; \sin \theta \; d\theta \; d\phi \quad . \qquad (3.1.2)$$

When we consider an extended target with a total number of nV atoms, where n is the number density and V is the volume, the total number of events is given by

$$Z = j \; Q \; n \; V \quad . \qquad (3.1.3)$$

An event is defined by the occurrence of a scattered electron, produced either elastically or inelastically. For an inelastic process, an event can also be defined by the occurrence of an excited atom. We shall be concerned mainly with this second possibility.

In an absolute measurement, according to (3.1.3), the total number of events or some known fraction of it must be determined and the density of the target must be known. For a measurement of the excitation function (the energy dependence of the cross section in arbitrary units) the knowledge of the target density is not necessary, provided it is held constant during the measurement. Absolute values can then be obtained by normalisation to theory or by measuring the ratio of two cross sections of which one

is known. In elastic cross section measurements, absolute values can also be obtained by making a phase shift analysis at a resonance for different scattering angles (Gibson and Dolder 1969), (Williams 1974).

3.2 Crossed Beam Technique

Scattering of electrons by the inert gases can be investigated using a static gas target at the rather high pressure of a few millitorr. A typical modern experiment of this type using high energy resolution is that by Sanche and Schulz (1973). However, when working with reactive gases, the crossed beam technique must be used, where an atomic beam is crossed by the electron beam.

Normally, the atom beam is formed by effusion from an aperture source, and since the number density in the beam drops as the inverse square of the distance from the source, the main problem one encounters is that of low target density and, consequently, of low signal. Often the density of the residual gas is higher than the beam density, and this may lead to a high level of background signal. In such cases the true signal can be picked out by mechanically chopping the beam and using phase sensitive detection. (Brackmann, Fite and Neynaber 1958).

Fite (1962) gives a detailed description of the techniques used in excitation cross section measurements, especially in atomic hydrogen. Heddle and Keesing (1968) review the techniques used in optical excitation measurements.

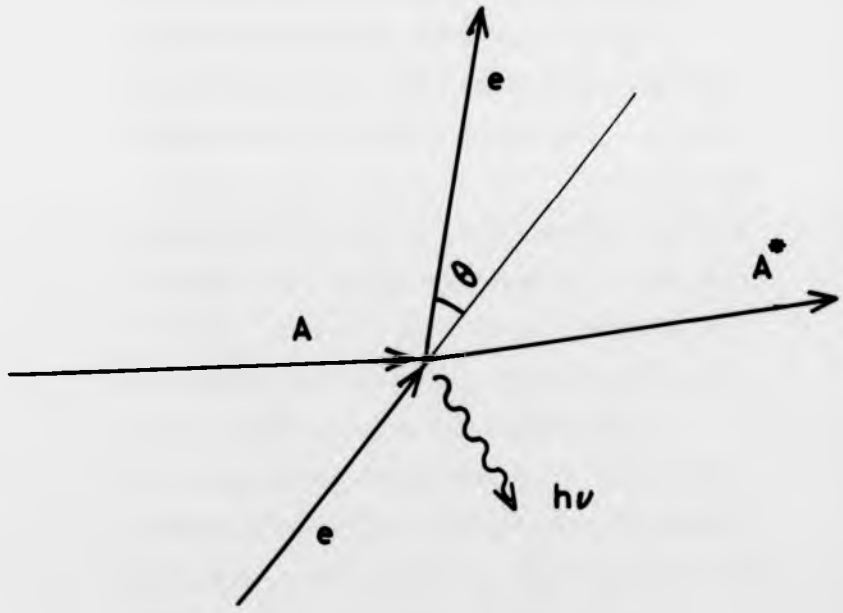

Fig. 3.1 Principle of crossed beam experiment.

Fig.3.1 shows the principle of a crossed beam experiment. The incoming atom beam A is bombarded, usually at right angles, by an electron beam. Scattering events can be detected,

1. by the emerging electrons, yielding the differential cross section $\sigma(\theta, \phi)$,
2. in the case of an inelastic event, by the presence of the excited atom A*. If the excited atom is short lived, then the photon emitted in the decay is detected. If the atom is long lived (metastable) it can be detected directly by surface detectors or by quenching, and this method yields the total cross section for excitation,
3. by beam recoil, which relies on the recoil suffered by the atom during the collision. An event is detected by a deflection of the atom out of its original direction.

The second method listed above has been used in this experiment.

3.3 Basis of Experiment

Fig.3.2 shows the term diagram of atomic hydrogen. The 2s-state is metastable since its decay into the ground state is forbidden by the selection rule $\Delta L = \pm 1$. Decay into the $p_{1/2}$ state can be neglected because of the extremely small energy separation (Lamb shift) corresponding to a transition frequency of about 1000 MHz. Experimentally, the lifetime of the metastable atoms is limited by collisions

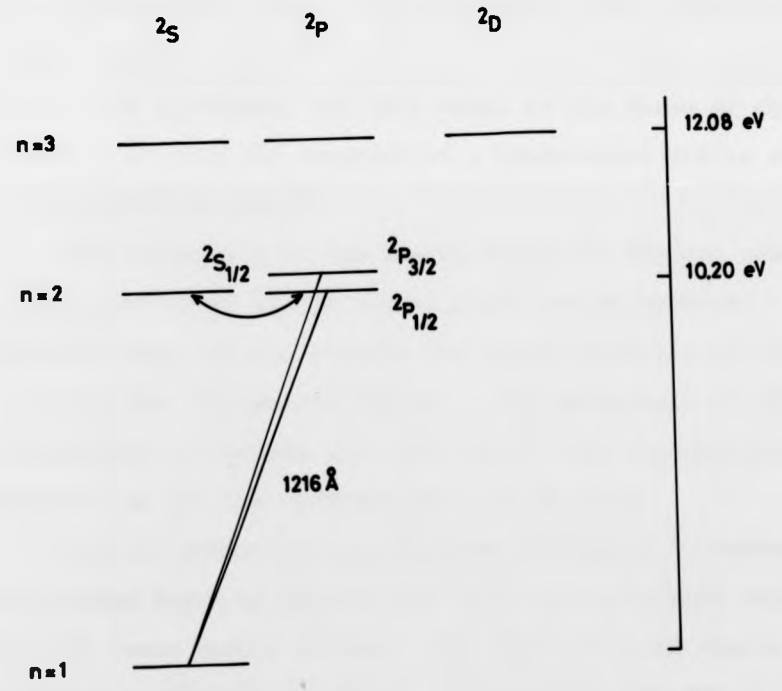

Fig. 3.2 Hydrogen term diagram, schematic.
The fine structure of the n=3 levels is not shown, while that of the n=2 levels has been exaggerated.

with residual gas atoms and ultimately by collisions with the walls of the system.

The long lifetime of the 2s-atoms is used to separate the 2s-atoms from the simultaneously excited 2p-state which decays in the interaction region, since its lifetime is only about 10^{-9} sec. The metastable atoms eventually enter a static electric field which causes Stark mixing of the 2s and 2p states, and this leads to the decay of the metastables with the emission of a Lyman-alpha photon at a wavelength of 1216 Å.

The excitation of the lowest states in krypton and xenon which decay to the ground state can be observed with the same set-up, placing the photon detector so that it views the interaction region. The wavelength of the transitions is between 1165 and 1469 Å, and the same photon detector as for the hydrogen case can be used.

Fig.3.3 shows the term diagram of krypton and xenon. The ground state of krypton has a $4p^6$ configuration with all the lower shells filled. The first excited states have the configuration $4p^5 5s$. The states with J=2,0 are metastable and the excitation of the J=1 states can be measured by counting the number of photons at 1236 and 1165 Å. The two lines were not resolved. From 10.03 to 10.64 in krypton and from 8.44 to 9.57 eV in xenon, however, excitation of the $^3P_1$ states alone is observed.

3.4 Experimental Approach

The first problem to be solved is that of building a hydrogen atom source of high intensity. Basically,

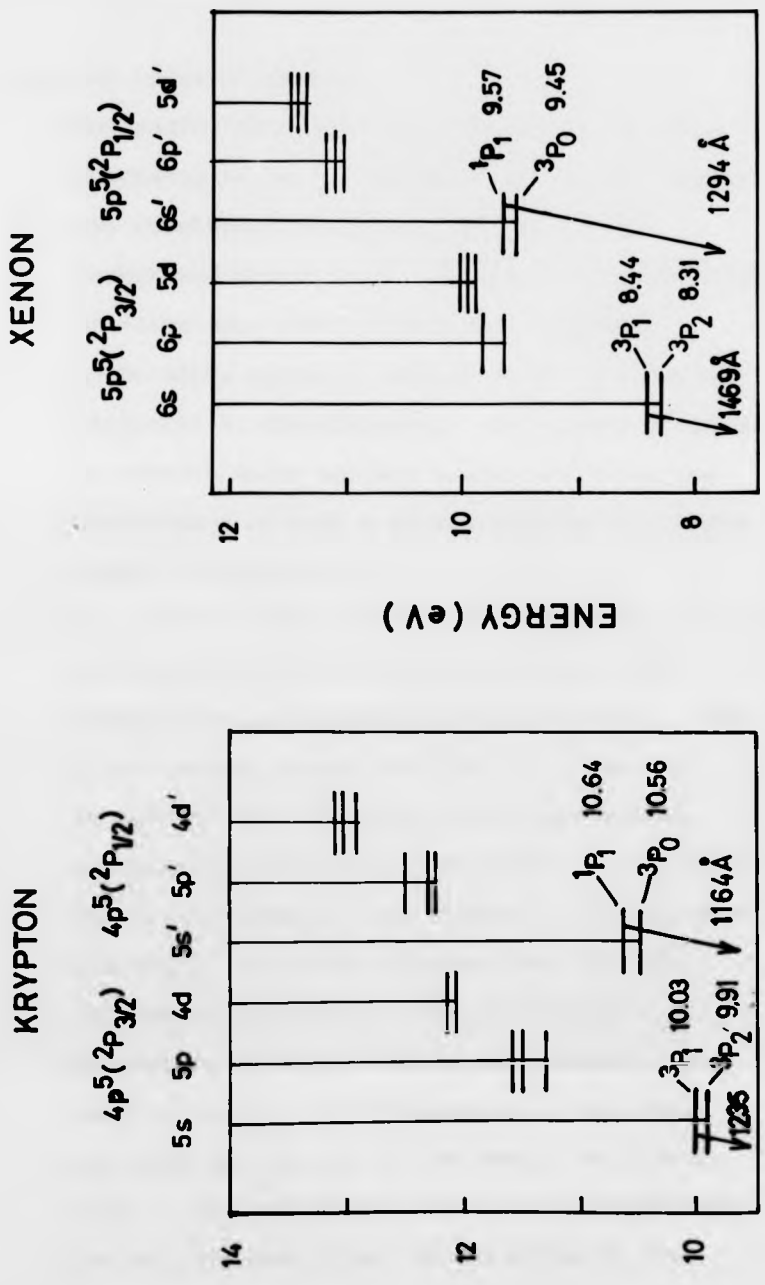

Fig.3.3 Krypton and xenon term diagram.

there are two types of sources.

1. The radio frequency discharge source, where a discharge is run in hydrogen gas. This source was considered unsuitable because of the background generated by the discharge, consisting of electrons, ions and photons, including Lyman-alpha photons, against which it would be difficult to discriminate. It is also difficult to operate under optimum conditions since the performance of such a source depends on a large number of parameters.
2. The thermal source (oven), which is easier to operate since the dissociation depends only on the temperature and pressure within the oven. The first thermal source for hydrogen (Lamb and Retherford 1950) consisted of a thin walled tungsten cylinder with a small hole in the wall. The disadvantage of this source is the low beam intensity, since the effusion from the hole follows a cosine law. The collimating properties of long channels can, however, be used to improve the performance of the oven, and this was the aim of the design described here. The same source could of course be used for all the rare gases, by operating at room temperature.

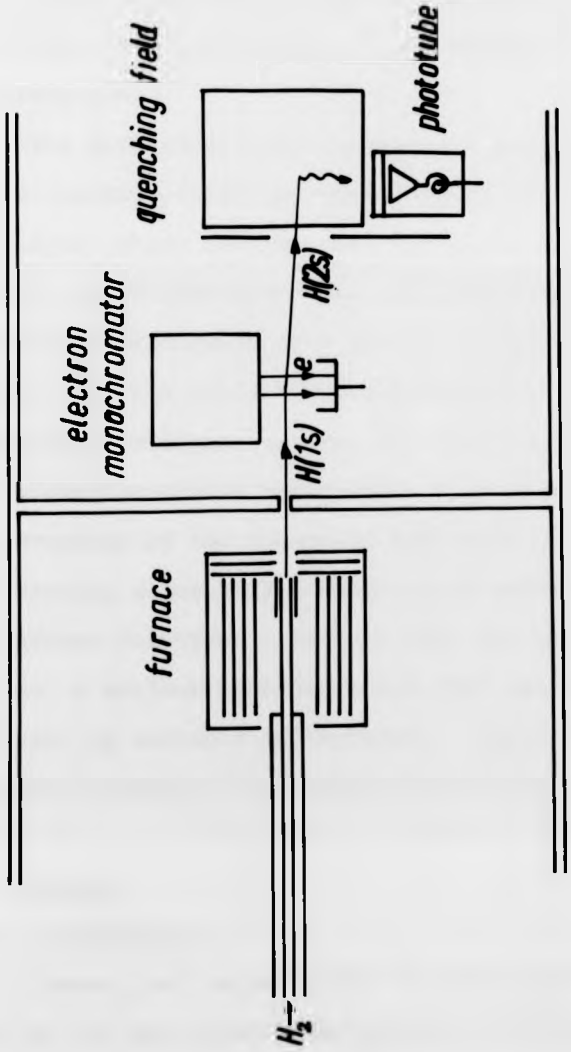

Fig.3.4 Schematic diagram of H(2s) experiment.

The next problem is that of building an electron monochromator. Only those velocity selectors using electric fields were considered, and the 127° cylindrical type (Marmet and Kerwin 1960) was preferred to the hemispherical type because of its simpler mechanical construction.

The detection of the metastable 2s-atoms by quenching in an electric field was preferred to the surface detection technique, where the internal energy of the 2s-atoms is used to eject electrons from a metallic surface. The latter detector would have had direct view of the interaction region and thus would have been bombarded by photons and scattered electrons, causing a high noise level, a problem not encountered with the quenching technique. The disadvantage of the quenching technique is its low efficiency, since only a small solid angle is covered by the photon detector. Photons from the interaction region are not a serious problem, since they can only reach the detector by multiple reflections. Fig.3.4 shows a schematic diagram of the experimental arrangement.

4. Theory

4.1 Introduction

Theoretical calculations of scattering cross sections have so far been restricted mainly to hydrogen, since it is only for this atom that exact wave functions and consequently, charge distributions which determine the interaction potential, are available. Even then,

approximations must be made to solve the scattering problem because of its three-body nature of proton + 2 electrons. The impinging electron distorts the atom during the collision and this process must be allowed for in the theory. In the Born approximation, the distortion is neglected, and this approximation can therefore only be employed at high incident energies. For the heavy rare gases only the Born approximation calculation has been carried out (Ganas and Green 1971).

The different approaches to solving the scattering problem have been covered in a number of textbooks and reviews (Mott and Massey 1965, Massey and Burhop 1969, Moiseiwitsch and Smith 1968) and only a brief summary of the main results is presented here.

In section 2 of this chapter some basic concepts are introduced, section 3 presents some aspects of the general theory of electron-hydrogen scattering, and section 4 deals with resonances.

4.2 Basic Concepts and Definitions

For a stationary beam of electrons impinging in the z-direction, the wave function describing the scattered electrons at large distances from the scattering centre is given by,

$$\psi(\vec{r}) \sim e^{ik_o z} + r^{-1} \sum_n e^{ik_n r} f_n(\theta, \phi) \qquad (4.2.1)$$

The first term is the incoming plane wave representing electrons of momentum $\hbar k_o$, the second term is the outgoing spherical wave and represents the scattered

electrons of momentum $\hbar k_n$ with $k_n = k_o$ for elastic scattering and $k_n < k_o$ for inelastic scattering, and $f_n(\theta, \phi)$ is the scattering amplitude.

The differential cross section as defined in (3.1.1) is related to the scattering amplitude by,

$$\sigma_n(\theta, \phi) = \frac{k_n}{k_o} |f_n(\theta, \phi)|^2 . \qquad (4.2.2)$$

The scattering problem is solved when a solution of the form (4.2.1) is found for the wave equation.

4.3 Theory of Electron-Hydrogen Scattering

Neglecting relativistic effects and spin-orbit interaction, the time independent wave equation for electron-hydrogen scattering is given by the Schrödinger equation,

$$\left[-\frac{\hbar^2}{2m} (\nabla_1^2 + \nabla_2^2) - \frac{e^2}{r_1} - \frac{e^2}{r_2} + \frac{e^2}{r_{12}} - E \right] \Psi(\vec{r}_1, \vec{r}_2) = 0, \qquad (4.3.1)$$

where E is the total energy of the system atom-electron, $\vec{r}_1$ and $\vec{r}_2$ are the position vectors of the atomic electron and impinging electron relative to the proton and $r_{12} = |\vec{r}_1 - \vec{r}_2|$ is the distance between the electrons. The usual theoretical approach is to expand the total wave function $\Psi(\vec{r}_1, \vec{r}_2)$ in terms of the eigenfunctions $\psi_\nu(\vec{r}_1)$ of the hydrogen atom

$$\Psi(\vec{r}_1, \vec{r}_2) = \sum_\nu F_\nu(\vec{r}_2) \psi_\nu(\vec{r}_1) , \qquad (4.3.2)$$

with

$$\left[-\frac{\hbar^2}{2m} \nabla^2 - \frac{e^2}{r_1} - E_\nu \right] \psi_\nu(\vec{r}_1) = 0 . \qquad (4.3.3)$$

The symbol ν represents the quantum numbers n,l,m and the

E_ν are the energy eigenvalues. The series (4.3.2) is an infinite one and should include integration over the continuum states.

Substituting (4.3.2) in (4.3.1), multiplying by $\psi_\nu^* (\vec{r}_1)$, and integrating with respect to $\vec{r}_1$, the coordinate of the atomic electron, one obtains the system of differential euqations,

$$(\nabla_2^2 + k_\nu^2) F_\nu (\vec{r}_2) = \frac{2m}{\hbar^2} \sum_{\nu'} V_{\nu\nu'} (\vec{r}_2) F_{\nu'} (\vec{r}_2), \quad (4.3.4)$$

where

$$V_{\nu\nu'} (\vec{r}_2) = \int \psi_\nu^* (\vec{r}_1) \left[\frac{e^2}{r_{12}} - \frac{e^2}{r_2} \right] \psi_{\nu'} (\vec{r}_1) \, d\vec{r}_1 , \quad (4.3.5)$$

and the E_ν are the energy eigenvalues of the hydrogen atom with

$$k_\nu^2 = (E - E_\nu) \, 2m/\hbar^2 . \quad (4.3.6)$$

The $V_{\nu\nu'}$ are known functions of $\vec{r}_2$. V_{oo} represents the mean interaction of the electron with the ground state atom. Only those solutions of (4.3.4) satisfying the boundary conditions (4.2.1) are wanted so that,

$$F_\nu (\vec{r}_2) \sim e^{i \vec{k}_o \vec{r}_2} \delta_{o\nu} + \frac{e^{i k_\nu r_2}}{r^2} f_\nu (\vec{r}_2) . \quad (4.3.7)$$

The coupled differential equations can then be simplified by the standard partial wave analysis, separating angular and radial variables.

Up to now, no provision has been made for electron exchange, and in order to do that, the wave function must be antisymmetric for exchange of the space and spin coordinates of the two electrons. Thus,

$$\Psi^{\pm} (\vec{r}_1, \vec{r}_2) = \frac{1}{\sqrt{2}} \sum_\nu \left[\psi_\nu (\vec{r}_2) F_\nu^{\pm} (\vec{r}_1) \pm \psi_\nu (\vec{r}_1) F_\nu^{\pm} (\vec{r}_2) \right], \quad (4.3.8)$$

where the wave functions $\underline{\Psi}^+$ and $\underline{\Psi}^-$ are associated with singlet and triplet scattering. For an unpolarized beam, the relative probability of the electrons being in antiparallel spin states is $1/3$, so that the mean cross section is given by,

$$\frac{1}{4} \left| f_\nu^+ (\theta, \phi) \right|^2 + \frac{3}{4} \left| f_\nu^- (\theta, \phi) \right|^2 . \qquad (4.3.9)$$

The substitution of the full antisymmetric wave function $\underline{\Psi}^\pm$ into the Schrödinger equation leads to a more complicated set of integro-differential equations, and this case will not be considered here.

In practice, only a small number of discrete states can be included in the expansion (4.3.2). It would seem that taking all the open channels should give a good approximation, but this is not the case, since the closed channels influence the scattering amplitude when the threshold of these channels is approached. The inclusion of the states with higher n is necessary to account for the polarizability of the atom, i.e. the distortion.

In the close coupling method, all the open channels and the lowest closed channels which are strongly coupled to the open channels are included in the expansion (4.3.2). The greater the number of channels that are retained, the greater the accuracy of the approximation. However, the amount of computer time increases rapidly with the number of eigenstates, and the most sophisticated close coupling calculation on hydrogen to date involved the inclusion of only the six lowest states. The full antisymmetric wave function has to be included in order to account for electron exchange, which has the effect of reducing the cross section in the vicinity of threshold compared with

the non-exchange calculation. The importance of including the higher states was shown by Burke (1963). The inclusion of these higher states also reduces the cross section for the production of the 2s and 2p states considerably.

Recently, Geltman and Burke have introduced the pseudo-state modification of the close coupling method, which allows explicitly for the polarizability of the higher states, including the continuum,by introducing a finite number of pseudo-states with non-physical energies (Geltman and Burke 1970).

4.4 Resonances

The most important result of the close coupling calculation is the prediction of resonances. They appear when the lowest energetically inaccessible states are included in the expansion, that is the n=2 states in elastic scattering and the n=3 states for excitation of the n=2 states. Comprehensive reviews of resonance scattering theory have been given by Smith (1966) and by Burke (1968).

Resonances can be explained as the formation of a compound state when the incoming electron attaches itself to the target atom to form a temporary negative ion which decays after about 10^{-13} sec by the emission of the electron.

Resonances are supported by excited states of the target atom and the situation for the system H+e is illustrated in Fig.4.1. When the interaction potential between the excited state and the electron is strong enough

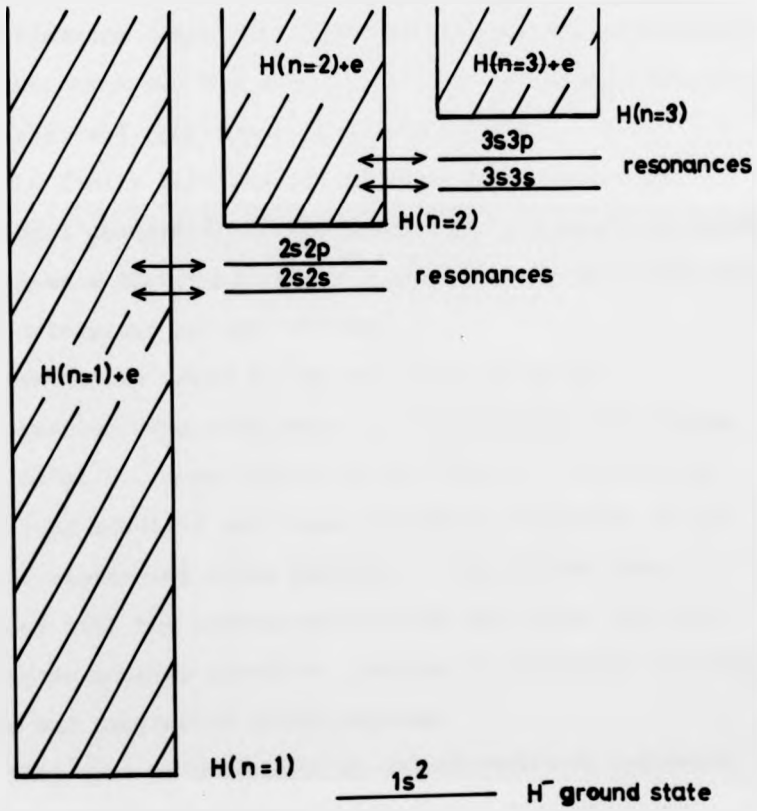

Fig.4.1 Resonances in e - H scattering.

to support a bound state of the negative ion, resonances are formed. They can be described as double excited states of H^-. Their energy position is usually a few tenths of an eV below the excited state, since the interaction between the core and the electron is small. The resonances cannot be stable because of the interaction with the continuum H+e with which they are always degenerate in energy, and they decay by autionization.

The finite lifetime of the resonances causes an additional phaseshift in the scattered wave and this leads to resonance structure in the cross section, with the width being determined by the lifetime.

Resonances based on the n=2 state have the configuration 2s2p,2s2p,2s3s, ... and similar resonances 3s3s, 3s3p, ... occur below the n=3 state. The former decay into H(n=1)+e and cause resonance structure in the elastic scattering cross section. The latter also interact with the continuum H(n=2)+e and decay into the n=2 states becomes possible, leading to resonance structure in the n=2 excitation cross section.

This type of resonance is called Feshbach resonance or closed channel resonance, since they lie below the excited state of the atom by which they are supported.

There is a second type of resonance, called a shape or open channel resonance, in which the electron is trapped by the penetrable barrier formed by the angular momentum of an electron with $L > 0$. Shape resonances often decay into the state by which they are supported, since they lie above them, and they often influence

excitation just above threshold.

As an illustration of Feshbach resonances, let us consider the case of elastic scattering in H under the assumption that the only other state which influences the scattering is the 2s-state. We thus have an idealized two-state system, and in this case the infinite system of coupled equations (4.3.4) reduces to two: *

$$(\nabla^2 + k_o^2)\, F_o\,(\vec{r}_2) = U_{oo}\,(\vec{r}_2)\, F_o\,(\vec{r}_2) + U_{o1}\,(\vec{r}_2)\, F_1\,(\vec{r}_2)\ , \tag{4.4.1}$$

$$(\nabla^2 + k_1^2)\, F_1\,(\vec{r}_2) = U_{o1}\,(\vec{r}_2)\, F_o\,(\vec{r}_2) + U_{11}\,(\vec{r}_2)\, F_1\,(\vec{r}_2)\ , \tag{4.4.2}$$

where $U_{nm} = U_{mn} = \frac{2m}{\hbar^2}\, V_{mn}$.

We now simplify by expanding in partial waves,

$$F_n\,(\vec{r}) = (k_n\, r)^{-1} \sum_{\ell} (2\ell + 1)\, G_{n\ell}\,(r)\, P_\ell\,(\cos\theta)\ , \tag{4.4.3}$$

where the P_ℓ are the Legendre polinomials.

This leads to the following equations for the radial functions G,

$$\frac{d^2 G_{o\ell}}{dr^2} + \left(k_o^2 - \frac{\ell\,(\ell+1)}{r^2} - U_{oo}\right) G_{o\ell} = U_{o1}\, G_{1\ell}\ , \tag{4.4.4}$$

and

$$\frac{d^2 G_{1\ell}}{dr^2} + \left(k_1^2 - \frac{\ell(\ell+1)}{r^2} - U_{11}\right) G_{1\ell} = U_{o1}\, G_{o\ell}\ , \tag{4.4.5}$$

with the asymptotic conditions

$$G_{o\ell} \sim 1^{\ell}\ \sin\,(k_o r - \tfrac{1}{2}\,\ell\pi) + \alpha_\ell\, e^{i\,k_o r}\ , \tag{4.4.6}$$

$$G_{1\ell} \sim \beta_\ell\, e^{i\,k_1 r}\ . \tag{4.4.7}$$

---

* In the following equations, the index 0 refers to the ground state and the index 1 refers to the 2s-state.

We now consider only s-wave scattering. If the energy of the incident electrons is below the n=2 threshold, the 2s-state cannot be excited and we get a negative k_1^2 in (4.4.5). Thus,

$$\frac{d^2G_o}{dr^2} + (k_o^2 - U_{oo})\, G_o = U_{o1}\, G_1 \quad , \qquad (4.4.8)$$

$$\frac{d^2G_1}{dr^2} - (K^2 + U_{11})\, G_1 = U_{o1}\, G_o \quad , \qquad (4.4.9)$$

where

$$-K^2 = k_1^2 = k_o^2 - \frac{2m}{\hbar^2}\,\Delta E < 0 \quad .$$

ΔE is the excitation energy of the 2s state and the fact that k_1^2 is negative shows that no real excitation takes place. We thus get an exponential decay for the 2s wavefunction,

$$G_o(r) \sim \sin k_o r + \alpha\, e^{i k_o r} \quad , \qquad (4.4.10)$$

$$G_1(r) \sim \beta\, e^{-Kr} \quad .$$

If we look at the homogeneous equivalent of equation (4.4.9), i.e. setting $U_{o1} = 0$

$$\frac{d^2 H_1}{dr^2} - (K^2 + U_{11})\, H_1 = 0 \qquad (4.4.11)$$

we notice that it is the equation for an electron under the influence of the mean potential of a 2s atom. Since the potential is attractive, there will be bound states of energy $-\hbar^2K_1^2/2m$, $-\hbar^2K_2^2/2m$, ... with wave functions X_1, X_2, ... If the coupling potential U_{01} were zero,

we would have two degenerate solutions of the wave equation. The first, solution of (4.4.8), which is given by $\psi_o(r_1)\, F_o(r_2)$ belongs to the elastic scattering continuum, while the second, solution of (4.4.9) with $U_{o1} = 0$, given by $\psi_1(r_1)\, X_j(r_2)$, is a discrete function corresponding to a doubly excited state of H^-.

The resonance arises because of the coupling between the two equations. If we expand G_1 in terms of the eigenfunctions of the homogeneous equation (4.4.11)

$$G_1 = \sum_j a_j X_j + \int a(E)\, X_E\, dE \quad , \qquad (4.4.12)$$

where X_E is a continuum wavefunctions of (4.4.11) corresponding to an energy $E = \hbar^2 k_E^2/2m$, with

$$\frac{d^2X_j}{dr^2} - (K_j^2 + U_{11})\, X_j = 0 \qquad (4.4.13)$$

$$\frac{d^2X_E}{dr^2} + (k_E^2 - U_{11})\, X_E = 0 \qquad (4.4.14)$$

we get, after substituting the expansion in (4.4.9) and using the two preceding equations

$$\sum_j (K_j^2 - K^2)\, a_j X_j - \int (k_E^2 + K^2)\, a(E)\, X_E\, dE = U_{o1}\, G_o \, . \qquad (4.4.15)$$

Multiplying by X_j^* and integrating over r we get,

$$a_j = \frac{\int X_j\, U_{o1}\, G_o\, dr}{K_j^2 - K^2} \quad , \qquad (4.4.16)$$

and

$$a_E = -\frac{\int X_E\, U_{o1}\, G_o\, dr}{k_E^2 + K^2} \, . \qquad (4.4.17)$$

Clearly, singularities occur whenever K^2 is equal to one of the K_j^2, corresponding to the bound states of the H^- ion, and these singularities lead to the resonance effects.

When investigating the resonance region, where $K^2 \simeq K_j^2$, the sum in the expansion (4.4.12) can be reduced to one term and a solution of equation (4.4.9) for G_0, which describes elastic scattering, can be found using a Green's function.

The partial cross section for s-wave scattering near the resonance is given by,

$$Q_o^{e\ell} = \frac{\pi}{k_o^2} \left| \frac{i\Gamma}{E - E_r + \frac{1}{2} i\Gamma} + e^{-2i\eta} - 1 \right|^2 , \quad (4.4.18)$$

where Γ is the width of the resonance which depends on the strength of the interaction between the bound state wavefunction and the continuum wavefunction, via the coupling potential U_{01}, $E = \hbar^2 k_o^2/2m$, $E_r = (2m\Delta E/\hbar^2 - K_j^2 + \Delta K_j^2)\,\hbar^2/2m$ is the resonance energy, and η is the phase shift due to potential scattering. Note that the resonance energy has been shifted by ΔK_j^2 from the bound state energy. This treatment has been given by Massey and Burhop (1969).

The first term in equation (4.4.18) is the resonance contribution, while the second term arises from the scattering by the mean potential of the atom. If the resonance term dominates,

$$Q_o^{e\ell} = \frac{\pi}{k_o^2} \frac{\Gamma^2}{(E - E_r)^2 + \frac{1}{4}\Gamma^2} . \quad (4.4.19)$$

This is the Breit-Wigner one level formula (Breit and Wigner 1937) which was derived originally to describe resonance phenomena in nuclear scattering due to the formation of compound states.

The Breit-Wigner formula has the shape of a resonance peak centered around E_r with a half width Γ. When the potential scattering is taken into account, interference between the two contributions occurs and this leads to a more complicated shape of the resonance depending on the phase shift η for potential scattering.

4.4.1 Results for Atomic Hydrogen

Fig.4.2 shows the results of the six state close coupling calculations (Burke, Ormonde and Whitaker 1967) and of the three state + 20 correlation terms calculation (Taylor and Burke 1967). The latter method allows explicitly for the interaction between the two electrons in a similar way as in the helium bound state problem. Also shown are the pseudo-state results (Geltman and Burke 1970), which give the best results for the absolute values of the cross section, since they satisfy the extremum principle for the phase shifts.

Just above the n=2 threshold, the cross section is dominated by a S=0, L=1 ^1P shape resonance at 10.222 eV with a width of only 0.015 eV, which is unusually narrow for a shape resonance.

The Feshbach resonances lie below the n=3 threshold, and their position and width is given in Table 4.1.

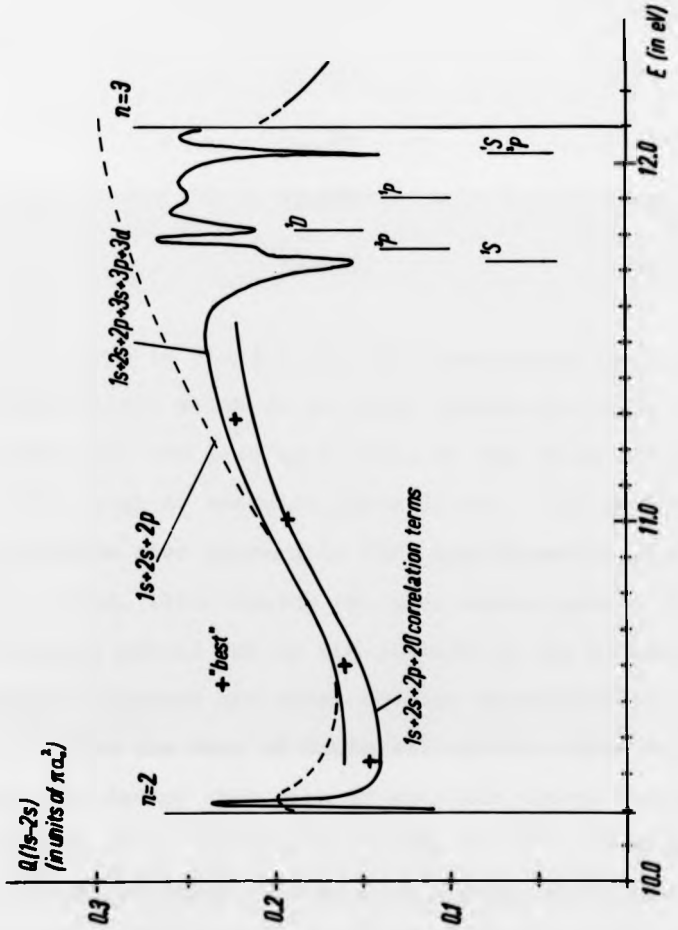

Fig.4.2 Close coupling results for the 1s-2s excitation cross section in H.

Table 4.1

Resonances below the n=3 threshold (Macek and Burke 1967)

State	Energy (eV)	Width (eV)
^1S	11.733	0.038
^1S	12.037	0.008
^1P	11.915	0.038
^3P	11.764	0.048
^3P	12.048	0.007
^1D	11.819	0.049

Also shown in Fig.4.1 are the three state close coupling calculations which do not show resonances below the n=3 threshold, and lead to a value of the cross section which is too high at energies above 11 eV. The shape resonance also appears in this approximation, but it is too broad, illustrating the poor convergence of the close coupling method due to the neglect of the higher states which influence the cross section considerably.

From the data of Table 4.1 and the curve of Fig.4.2 one can deduce that with an electron energy resolution of 100 meV it is possible to detect the $^1S + {}^3P$ resonances at 11.73 eV which overlap with a total width of about 80 meV. The shape resonance at threshold can only be detected provided the signal-to-noise ratio is very good

with this energy resolution. The other resonances close to the n=3 threshold are too narrow to be detected.

4.4.2 Theoretical Results for the Heavy Rare Gases

Since the close coupling method requires the knowledge of the target wave functions, it cannot easily be applied to the heavier atoms, except in helium, where good approximate wave functions are available.

The excitation of the heavy rare gases has only been studies in the Born approximation, (Ganas and Green 1971) and this work has been extended to lower energies for argon and neon using the distorted waves approximation (Sawada, Purcell and Green 1971).

For krypton and xenon, no theoretical results applicable to the threshold region exist.

5 The Apparatus

5.1 The Vacuum System

The experimental apparatus is shown in Fig.5.1. Its design considerations were based on its application as an atomic hydrogen beam apparatus and alterations for the rare gases will be mentioned when necessary. The vacuum system consists of two differentially pumped chambers, the oven chamber and the excitation chamber. The first chamber houses the high temperature hydrogen oven, which acts as a source of atomic hydrogen. The second chamber houses the electron monochromator and the detector, consisting of the electrostatic quench field and the photon counter. The two chambers are separated by a vacuum wall with the collimation aperture for the atom beam.

Hydrogen being a non-condensible gas, large diffusion pumps were employed in order to obtain an intense atom beam with a low background of molecular gas, which is formed by recombination of the atoms on the walls of the chambers. Oil diffusion pumps with speeds of 6000 l/sec (for air) for the oven chamber and 3000 l/sec for the excitation chamber were used. A two-stage rotary pump with a speed of 100 m^3/h was used as forepump.

The two chambers could be isolated from the pumps by pneumatically operated gate valves which safeguard the system against backstreaming of oil in case of a power failure. An interlock system ensures that the valves are closed and the vacuum system is switched off in the case of a major vacuum leak, failure of the cooling water supply or failure of the liquid nitrogen supply for the diffusion pump

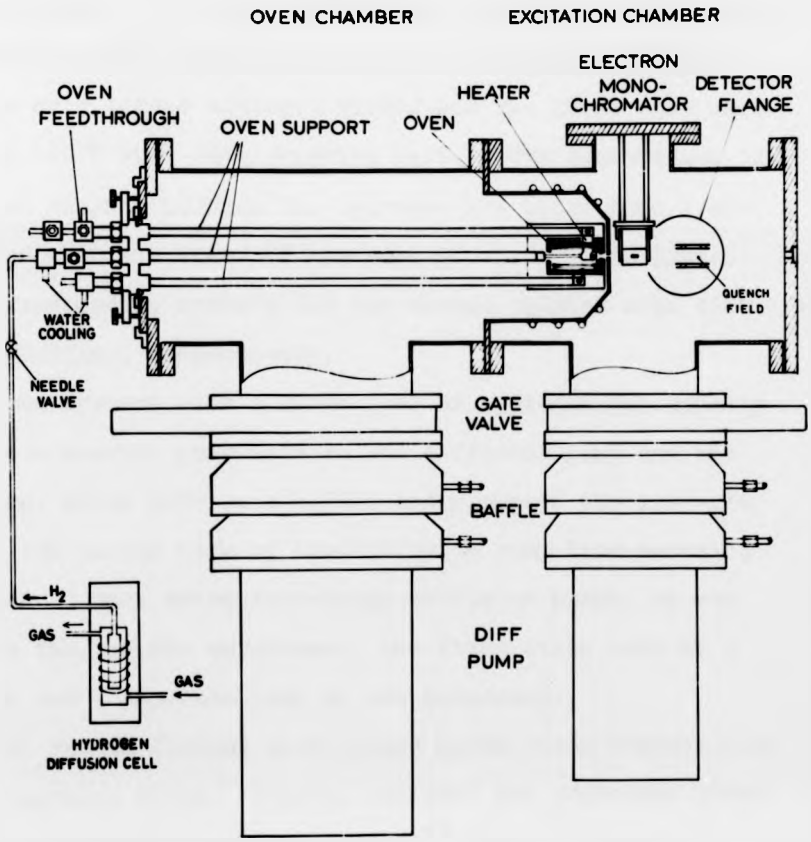

Fig.5.1 Atomic beam apparatus.

baffles. Although the vapour pressure of the diffusion pump oil (silicon oil DC 705) is less than 10^{-9} Torr, insulating layers can still be formed on the electrodes of the monochromator, if no precautions are taken against the backstreaming of oil vapour. Two high conductance baffles in series were used between the pumps and the vacuum chambers, the upper baffles were liquid nitrogen cooled and the lower ones were kept at -20°C by a refrigerating unit. The conductance of the oven chamber baffles for hydrogen was about 8000 l/sec, compared with the speed of the pump of about 12000 l/sec. The corresponding numbers for the second chamber were 4500 l/sec and 6000 l/sec, respectively.

Vacuum systems with a large load of hydrogen gas usually require a booster pump between the diffusion pump and the forepump, which acts as a buffer and prevents the pressure at the low vacuum side of the diffusion pump from becoming too high. When using four-stage diffusion pumps, as was done in the present experiment, the first stage acts as a booster and a separate pump is not necessary.

All vacuum flanges were sealed using viton O-rings with low outgassing rates. Typical residual gas pressures under no load conditions were less than 10^{-7} Torr. With the hydrogen beam on, the pressure rose to about 7×10^{-5} Torr in the oven chamber and 3×10^{-6} Torr in the excitation chamber. Diffusion of gas through the aperture between the chambers because of the pressure difference plays a major role in increasing the gas load of the excitation chamber. An additional buffer chamber would overcome this problem, it would however mean a loss in beam intensity because of the

increase in the distance from the beam source to the interaction region.

The two chambers were suspended from a metal beam using castor wheels so that the chambers and the two heavy end-flanges could be moved along the axis of the apparatus giving easy access to the interior.

5.1.2 The Oven Chamber

The cylindrical oven chamber with a diameter of 350 mm and a total length of 600 mm was made from stainless steel, and welded on the inside only to prevent trapped leaks. The length is mainly determined by the diffusion pump diameter of 350 mm.

This chamber houses the hydrogen oven with its support, and the electrical and water feedthroughs which are mounted on the big end-flange. Six additional flanges with diameters of 50 mm were used for the foreline bypass, the air admittance valve, the Pirani gauge and the ionization gauge.

The oven assembly was supported by four stainless steel tubes with a diameter of 16 mm. The central portion of the flange was sealed with a neoprene bellows and it could be adjusted by setting screws, moving the oven horizontally and vertically. The support rods consisted of two concentric tubes to carry the cooling water and they were electrically insulated from the flange by PTFE bushes, so that they could also be used as electrical feedthroughs. The centre tube carried the gas to the oven, and it was also water cooled. Fig.5.2 shows the oven flange with the oven support.

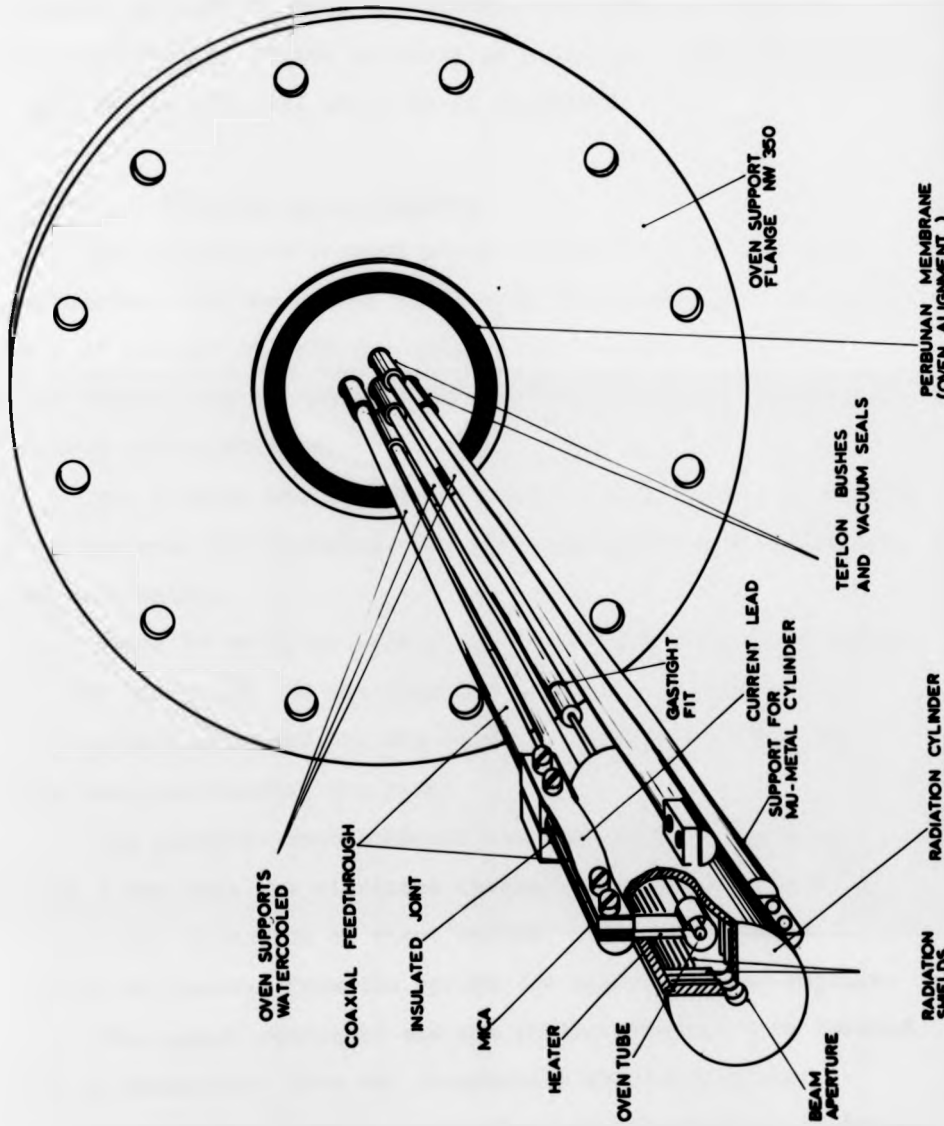

Fig.5.2 Oven flange with hydrogen oven.

The partition wall between the two chambers was dome shaped in order to make the distance between the oven and the interaction region as small as possible. The collimating aperture in the wall was 6 mm in diameter.

5.1.3 The Excitation Chamber

The excitation chamber which housed the electron monochromator, and the quench field with the Lyman-alpha detector, was of similar cylindrical shape with a length of 400 mm. The chamber was connected to the diffusion pump by the bottom flange with a diameter of 250 mm.

The chamber had two 150 mm ports for the detector assembly and the mass spectrometer, and a 200 mm port for the electron monochromator.

Three 50 mm ports were provided for the ionization gauge, the Pirani gauge and the foreline bypass. An additional 100 mm port was used for the cooling water feedthrough for the dome surrounding the oven.

The electron monochromator was mounted on a table in such a way that the electrons crossed the atom beam in a horizontal direction at right angles. The table could easily be removed from the system for inspection and repairs.

The quench condenser and the photon detector were located 100 mm downstream from the interaction region with the condenser plates horizontal and the detector parallel to the plates overlooking the space between the plates. The detector-quench field assembly was mounted on the detector flange, which is parallel to the plane of the drawing.

An observation window in the centre of the end flange

was used to align the oven with respect to the electron monochromator and the detector assembly using a telescope. The oven temperature was also monitored through this window with an optical pyrometer.

The chambers could be baked by a heating jacket to about 120°C which is the limit to which the viton O-rings can be heated.

5.1.4 Gas Handling System

The gas handling system, which avoids the use of high pressure hydrogen cylinders and the dangers associated with it, is also shown in Fig.5.1. A silver-palladium diffusion cell, heated to 350°C, is used as a hydrogen leak and supplies high purity hydrogen to the beam source. Town gas, containing about 40% hydrogen is fed to the cell and only hydrogen can diffuse to the vacuum side of the cell. Since a continuous flow of raw gas is necessary, the surplus gas is fed to a burner. The flow of hydrogen to the oven was controlled by a needle valve. In the case of the rare gases, the diffusion cell was replaced by a low pressure vessel containing research grade gas.

5.2 The Atom Beam Source

5.2.1 Beam Formation

In order to obtain an intense hydrogen atom beam, two conditions have to be fulfilled.

1. The dissociation of the beam should be as high as possible, and this depends mainly on the temperature in the oven and also on the pressure

in the source. Temperatures of 2600°K are necessary if a dissociation of more than 80% is to be obtained at a source pressure of about 0.1 Torr (Lamb and Retherford 1950).

2. The beam emerging from the source should be strongly peaked in the forward direction. A simple aperture source has the disadvantage of a broad cosine distribution of intensities, and it was decided to exploit the collimation properties of long channels.

The stationary flow and pressure characteristics of the beam apparatus are shown schematically in Fig.5.3. The relation between the total effusion rate N_o and the pressure p_o in the oven chamber is given by

$$N_o = 3.54 \times 10^{19} S_o p_o \quad . \qquad (5.2.1)$$

The numerical factor converts the flow rate in Torr l/sec into molec/sec, S_o is the pumping speed in l/sec and p_o is in Torr.

The pumping speed S_o is estimated using the manufacturers data, and all the numbers given in this paragraph are therefore only rough estimates. The intrinsic speed S_p of the pump for H_2 is not well known and was assumed to be 12000 l/sec, twice the speed for air. The resulting speed S_o is strongly dependent on the baffle conductance C according to the expression,

$$S_o = \frac{C}{1 + C/S_p} \quad , \qquad (5.2.2)$$

Since C, the conductance of the baffles, is approximately 8000 l/sec, a change of a factor of 2 in S_p only changes

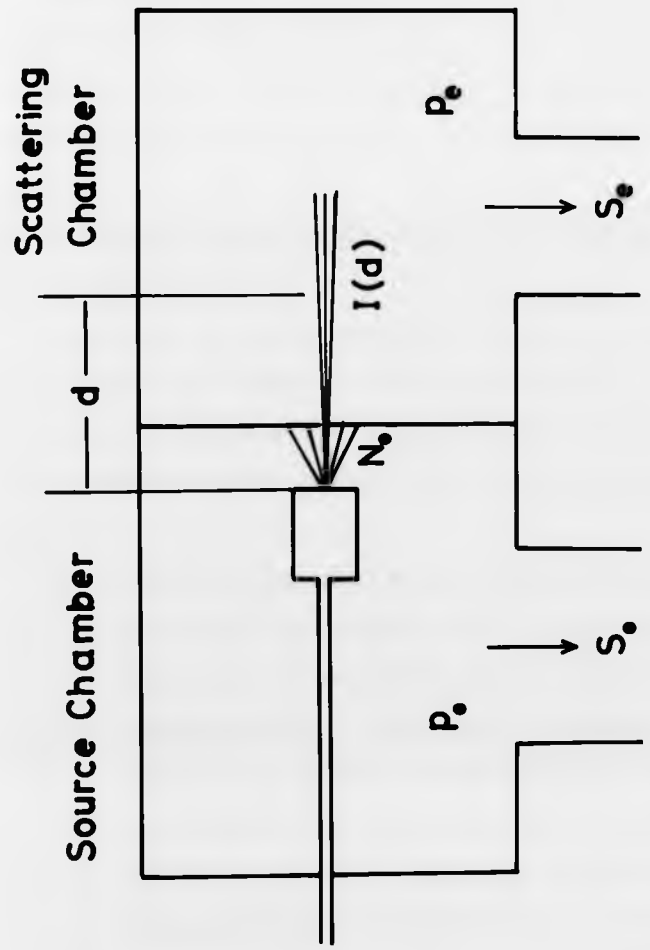

Fig.5.3 Gas flow in two-chamber apparatus, schematic.

S_o by 25%. According to (5.2.2) the pumping speed S_o is 5000 l/sec. With an oven chamber pressure of 10^{-4} Torr the total flow according to (5.2.1) is,

$$N_o = 1.7 \times 10^{19} \text{ molec sec}^{-1}.$$

The collimation properties of long channels have been studied theoretically by Clausing (1930) and experimentally by Becker (1961). These results were estended to higher pressures, where the flow is no longer molecular, by Giordmaine and Wang (1960). They showed that the beam properties are strongly dependent on the pressure conditions within the channel.

According to the relationship between the mean free path λ in the tube, its radius a, and its length L, different results for the beam intensity and angular distribution are obtained. It is assumed throughout that $a \gg L$ i.e. that the tube is long.

1. The limiting case at low pressures is that of molecular flow where $\lambda \gg L$, collisions between atoms can be neglected and the tube is called "transparent". This case is simplest from the theoretical point of view and gives the highest collimation, but the throughput is limited by the condition $\lambda \gg L$. The beam collimation is determined by the geometry of the tube.
2. At higher pressures, collisions between the atoms occur and play a major role in determining the beam characteristics. In the case $\lambda < L$, but with $\lambda > a$ at the low pressure end of the tube, the beam intensity can still be calculated.

This case is called "intermediate" flow.

The intermediate flow is the most important for practical applications, since transparent sources are limited to flow rates of the order of 10^{16} molec sec^{-1}.

Giordmaine and Wang (1960) calculated the beam intensity on the axis $J(\theta = 0)$, under the assumption of intermediate flow for a long tube and found,

$$J(\theta = 0) = \frac{3^{\frac{1}{2}} c^{\frac{1}{2}} a^{\frac{1}{2}} N^{\frac{1}{2}}}{2^{\frac{1}{4}} 8 \pi^{\frac{1}{2}} \sigma} \text{ molec sterad}^{-1} \text{ sec}^{-1}, \quad (5.2.3)$$

where c = mean velocity in cm/sec,

a = radius of tube in cm,

N = total flow molec/sec,

σ = molecular diameter, related to the collission cross section q by $q = \pi \sigma^2$.

The axial beam intensity is no longer proportional to the total flow rate N as it would for a transparent tube. The reason for this is the occurrence of collisions between the molecules in the tube, and this is illustrated by the fact that the molecular diameter appears in the formula. When the flow is increased the beam spreads, and a smaller proportion of the total flow is in the forward direction. For half width of the beam, i.e. the angle $\theta_{\frac{1}{2}}$ for which the intensity drops to half its maximum value at $\theta = 0$, Giordmaine and Wang give the result,

$$\theta_{\frac{1}{2}} = \frac{2\, 2^{\frac{1}{4}}\, 3^{\frac{1}{2}}\, \sigma\, N^{\frac{1}{2}}}{1.78\, a^{\frac{1}{2}}\, c^{\frac{1}{2}}} . \quad (5.2.4)$$

In this experiment the tube radius was 2 mm and the length was 100 mm. In order to determine the kind of flow that prevailed under the experimental conditions, the following

simple estimates were made.

The number density of the beam when emerging from the source is given approximately by,

$$n_o = \frac{N}{c\,A}, \qquad (5.2.5)$$

where c is the molecular velocity and A is the area of the source opening. With $a = 2 \times 10^{-1}$ cm and $c = 4 \times 10^{5}$ cm/sec equation 5.2.5 leads to a number density n_o of about 10^{14} molec/cm^3 at the exit of the source. The corresponding mean free path is given by

$$\lambda = (n\,q\,\sqrt{2}\,)^{-1}, \qquad (5.2.6)$$

where q is the molecular collision cross section. Thus the free path is about 4 cm, and, clearly, the condition for molecular flow, namely, that $\lambda \gg L$, is not fulfilled since in the experiment L = 10 cm. However since a = 0.2 cm, $\lambda > a$ at least at the end of the tube, and the conditions of intermediate flow are expected to apply.

The half width of the beam according to equation (5.2.4) is $\theta_{\frac{1}{2}} = 35^{\circ}$ compared with 60° for a simple aperture source with a cosine distribution. For the beam flux density I(d) in the interaction region at a distance of d = 10 cm from the source one obtains from Giordmaine and Wang's equation (5.2.3),

$$I(d) = J(0)/d^2 = 6 \times 10^{16} \text{ molec cm}^{-2} \text{ sec}^{-1}.$$

The corresponding number density in the beam is,

$$n = I / c = 10^{11} \text{ molec cm}^{-3}.$$

With these numbers, it is now possible to compare the number density of the beam, to which the signal will be proportional, with the density of the background gas due to the gas load, which is mainly molecular hydrogen. The

gas load of the excitation chamber has two causes, the first is the beam itself and the second is diffusion from the oven chamber because of the pressure differential. The first contribution is given by,

$$N_{beam} = J(0)\,\Delta\Omega = 7\times10^{18}\ 10^{-2} = 7 \times 10^{16} \text{ molec sec}^{-1},$$

where $\Delta\Omega = 10^{-2}$ is the solid angle subtended by the collimating aperture as seen from the beam source. The second contribution is given by

$$N_{diff} = \frac{3.5 \times 10^{22}\ \Delta p\, A}{\sqrt{MT}} = 5\times10^{16} \text{ molec sec}^{-1},$$

where Δp is the pressure difference between the chambers and A is the aperture area.

The total flow is therefore,

$$N_{tot} = 1.2 \times 10^{17} \text{ molec sec}^{-1},$$

which corresponds to a flow of 4×10^{-3} Torr l/sec. With a pumping speed of about 3000 l/sec for the excitation chamber, the background pressure due to the load will be 1.3×10^{-6} Torr. This pressure corresponds to a density of about 5×10^{10} molec cm^{-3}.

Comparing this density with the beam number density of about 10^{11} molec cm^{-3} it can be seen that they are roughly the same.

It can, however, be expected that the residual H_2 gas will not give rise to a high level of background, since the production of metastable H-atoms by dissociative excitation of H_2 has a threshold of 15 eV, well above the energy range of interest in this experiment. The production of countable ultraviolet radiation from excitation of the

H_2 molecule should not be a serious problem since the detector does not view the interaction region.

Collisional quenching of the metastable atoms by residual H_2 gas can be estimated using data of Fite, Stebbings and Brackmann (1959). With their value for the quenching cross section of 7×10^{-15} cm^2 for H_2 and a H_2 density of 10^{11} molec cm^{-3}, the mean free path for metastable atoms in the apparatus is 10 m, and this means that 99.3% of the metastables survive after travelling 8 cm, which is the distance from the excitation region to the detector.

5.2.2 Mechanical Design of the Oven

Having decided to use a long tube, a method of heating has to be devised. To obtain a high degree of dissociation in the beam, temperatures in excess of 2000°K have to be achieved. Lamb and Retherford (1950) calculated the dissociation of hydrogen in termal equilibrium with the oven walls as a function of temperature and pressure. At 2200°K and a pressure of 10^{-1} Torr the dissociation fraction is 80%. Tungsten is the only material that can be safely employed at these temperatures, and the major technical problem is that of achieving these high temperatures.

Electron bombardment of the source has often been used for this purpose and this is perhaps the most versatile method of heating since sources made of massive material can be used, either single channel or multichannel. In this technique, the oven is bombarded by electrons of 1-2 keV energy emitted from a filament surrounding it. The disadvantage of this method is that it produces a high

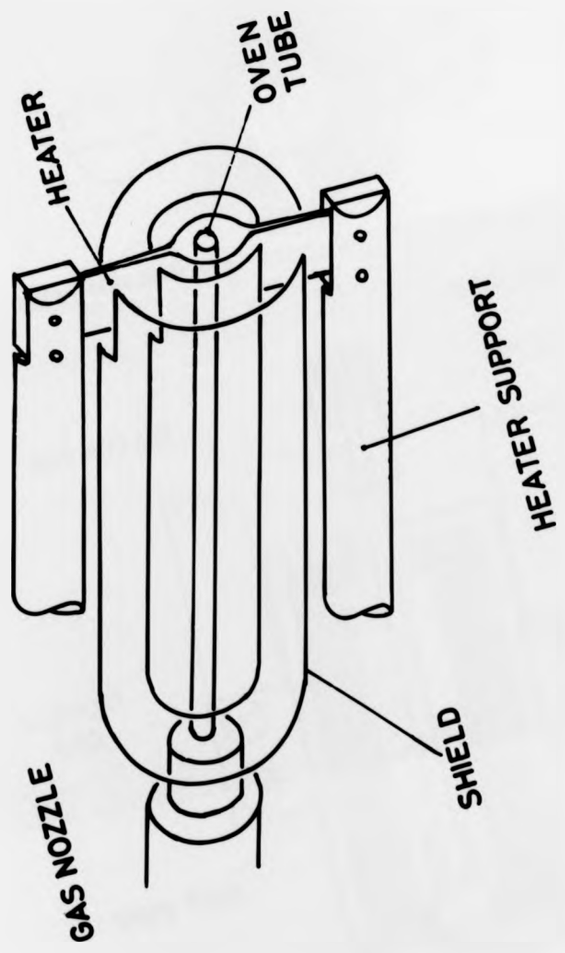

Fig.5.4.a. Hydrogen oven, preliminary heater arrangement.

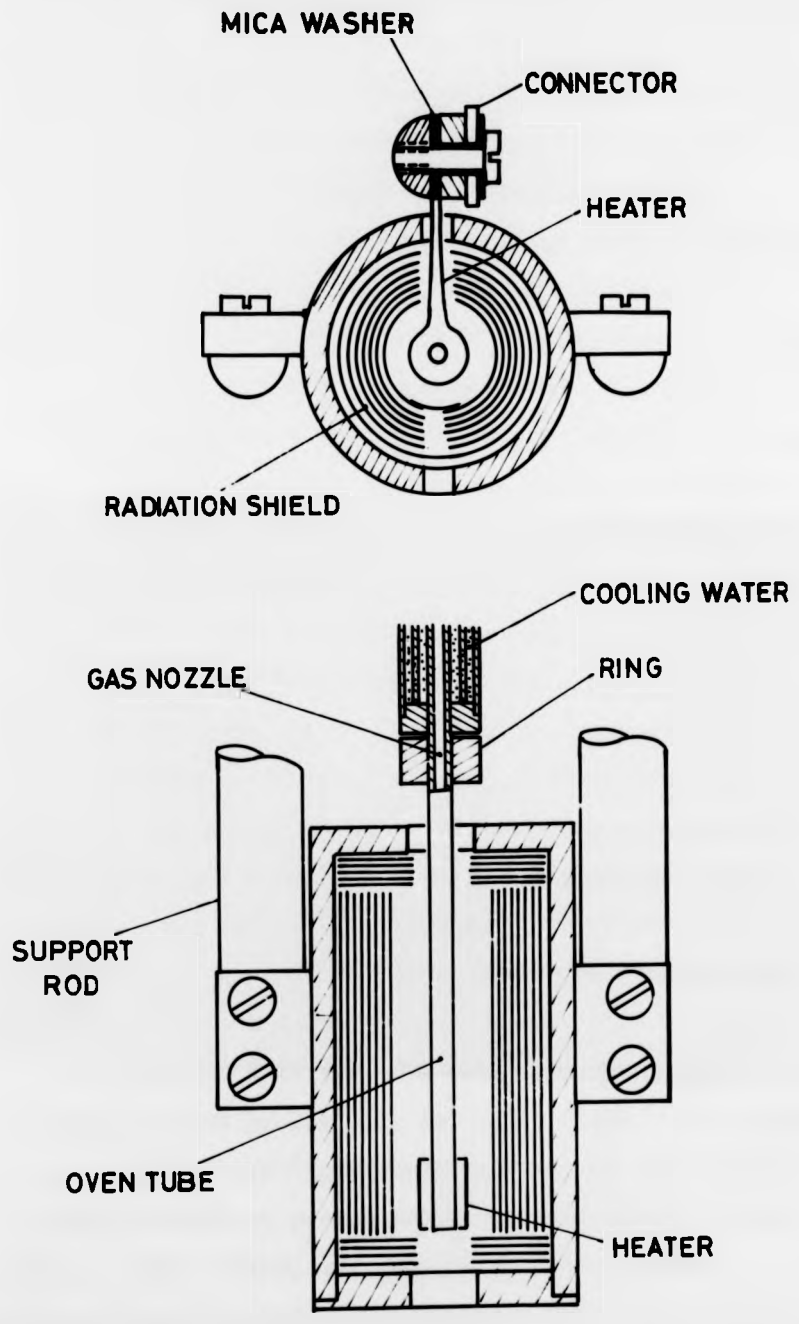

Fig.5.4.b. Hydrogen oven, final version.

background of Lyman-alpha radiation due to excitation of the residual H_2 gas in the oven chamber by the high energy electrons. (Hils, Kleinpoppen and Koschmieder 1966).

Resistance heating of the source was first employed by Lamb and Retherford (1950). A thin walled tungsten cylinder, closed at both ends, with a small aperture for the beam in the wall was used. A high current was passed through the tube, heating it to 2700° K. The disadvantages of this type of oven are the poor collimation properties and low beam flux density. There is, however, no ultraviolet background associated with this source.

The method adopted here uses heating by radiation which combines low ultraviolet background with good collimation by the use of a long tube. The heater, a tungsten ribbon, is separate from the tube and energy is transferred by radiation. This method is not as efficient as electron bombardment or direct heating and heat losses have to be minimized. The wall of the tube was made as thin as technically possible and extensive radiation shielding was provided.

Figs.5.4a and 5.4b show the oven with the heater arrangement in its preliminary and final forms. The heater, which is at about 3000°K, enclosed the tube at the open end. The first arrangement proved to be unsatisfactory for two reasons. When heated, the ribbons tended to flatten because of the attractive force between them, crushing the tube. Furthermore, this arrangement had a high stray magnetic field. In the final arrangement, shown in Fig.5.4b, a circular loop with the current flowing in opposite

directions along the straight legs was used. This heater was much more stable mechanically and it also had a much smaller stray magnetic field, especially since a coaxial current feed through was used.

The tube was made from tungsten foil 0.025 mm thick, the tube diameter was 4 mm and its length was 100 mm. The tungsten foil was bent in a special jig at a temperature of 700°C. The tube was fitted on to the gas nozzle and compressed by a closely fitting ring, in order to prevent gas leaking at this point.

The open end of the tube was enclosed by the tungsten ribbon heater with a thickness of 0.15 mm and a width of 15 mm. The heater was shaped in the form of a loop, with a total length of 80 mm. In order to minimise radiation losses, the heater was surrounded by a set of 8 concentric cylindrical radiation shields. The two inner ones were made of tungsten, to withstand the high temperature of the heater, the outer ones were made of molybdenum. The cylinders were spaced by indentation distributed over their surface. The radiation shield was housed in a stainless steel cylinder supported by the two water cooled rods.

The tungsten ribbon was bent in a jig at a temperature of about 700°C. This process relieved mechanical strain in the material. The maximum power dissipated in the heater was 1500 watts, at a current of 150 amps.

The coaxial feedthrough for the heater presented some major technical problems since it had to be water cooled and the inner and outer conductor had to be insulated from each other. At the same time, the insulation had to provide

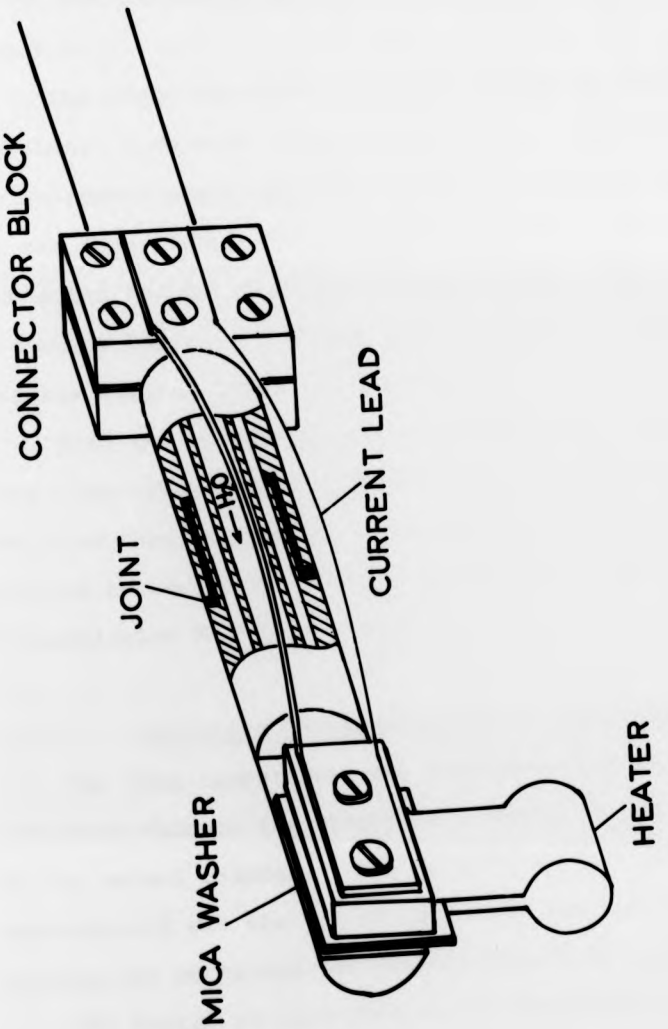

Fig.5.5. Coaxial heater feedthrough.

a vacuum tight seal, but the low vapour pressure resin that was used tended to crack under thermal stress when the oven was heated (Torrseal, Varian Vacuum). The final version which was strong enough to withstand the stress is shown in Fig.5.5.

The inner and outer tube act as the two conductors, insulated from each other at the joint. The heater is sandwiched between the tube connector, which is connected to the inner tube, and a stainless steel plate, which is connected to the outer tube by the copper lead and the connector block. A mica washer acts as an insulator between the two halves of the heater.

With two concentric mumetal cylinders enclosing the oven, the stray magnetic field in the interaction region was less than 20 mgauss. The earth's magnetic field was reduced to less than 10 mgauss by a set of three mutually perpendicular Helmholtz coils.

5.2.3 Operating Characteristics of the Hydrogen Oven

The oven temperature was monitored with an optical pyrometer through the observation window in the end flange of the second chamber. The reference point for these measurements was the tip of the oven, and the temperature reading was corrected for the emissivity of tungsten.

The degree of dissociation was determined with a commercial quadrupole mass spectrometer. The mass spectrometer was fitted with a crossed beam ionizer with an open interaction region in order to allow unimpeded access of the beam, and the ionizer was crossed with the

atom beam at the location of the electron monochromator. The dissociation was measured by comparing the height of the peaks of mass one and mass two.

The experimental problem that had to be overcome was the existence of a spurious mass one peak and the separation of the mass two signals arising from the residual H_2 gas and from the beam. This was done using phase sensitive a.c. detection techniques. For this purpose, the beam was mechanically chopped and the a.c. signal was compared with a reference signal from a photocell monitoring the position of the chopper. Only those components of the signal which are in phase with the reference and which represent the true beam signal are then amplified by the lock-in detector.

The dissociation is usually defined as the ratio of the number of molecules that have been dissociated to the total number of molecules. (Fite and Brackmann 1958). If N_1 is the number of atoms and N_2 is the number of molecules, then the number of dissociated molecules is $N_1/2$ since 2 atoms are produced for every molecule that is dissociated. From the above definition, it follows that the dissociation D is given by,

$$D = \frac{N_1/2}{N_1/2 + N_2} = \frac{1}{1 + 2N_2/N_1} . \qquad (5.2.8)$$

The mass spectrometer signal is proportional to the number density in the beam of the atoms and the molecules, respectively, and D can be written in the form,

$$D = \frac{1}{1 + \sqrt{2}\ S_2Q_1/S_1Q_2} . \qquad (5.2.9)$$

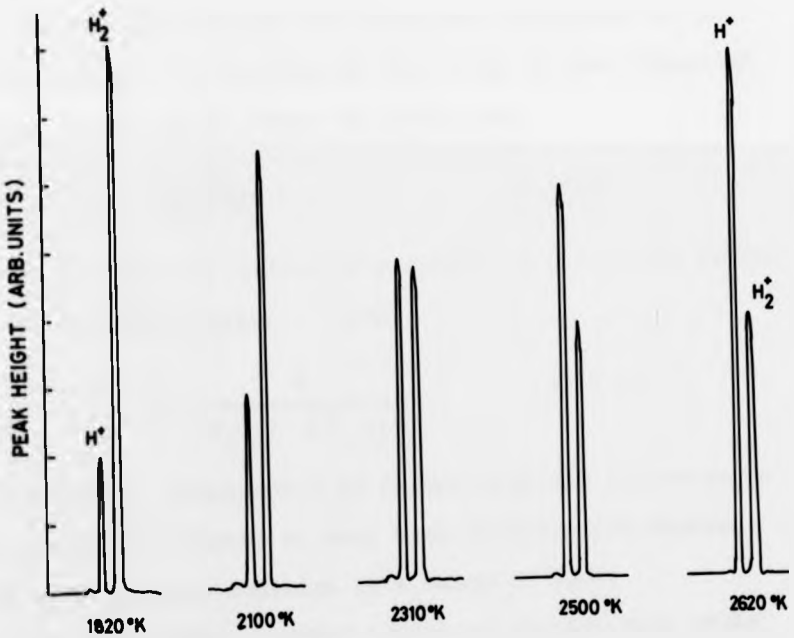

Fig.5.6.a. Mass spectrometer signal as a function of temperature.

S_1 and S_2 are the mass one and mass two signals, and Q_1 and Q_2 are the ionization cross sections for H and H_2 at the ionizer energy. Only the ratios of these quantities are required. The beam shapes for H and H_2 and the collection efficiencies of the mass spectrometer for H^+ and H^+_2 are assumed to be equal.

One can also define the fractional abundance X, of atomic hydrogen in the beam as the ratio of the number of H-atoms to the total number of particles,

$$X = \frac{N_1}{N_1 + N_2} . \qquad (5.2.10)$$

The two definitions differ by a factor of two in the second term of the denominator. Thus,

$$X = \frac{1}{1 + S_2 Q_1 / \sqrt{2}\ S_1 Q_2} . \qquad (5.2.11)$$

The fractional abundance X is larger than the dissociation D by about 10%, except at very high dissociation degrees, where both of them converge to a value of 100%.

Fig.5.6a shows recorded traces of the two mass peaks as a function of oven temperature. The dissociation D has been evaluated according to equations (5.2.9), with the ratio of the ionization cross sections $Q_1/Q_2 = 0.67$ at the ionizer energy of 90 eV (Fite and Brackmann 1958). Fig.5.6b shows the results for the dissociation as a function of temperature with the oven chamber pressure as a parameter. The fractional abundance X is about 10% higher. At a temperature of $2500^{\circ}K$ and a pressure of 6×10^{-5} Torr the dissociation exceeded 80%, with a fractional H-atom abundance of 90%.

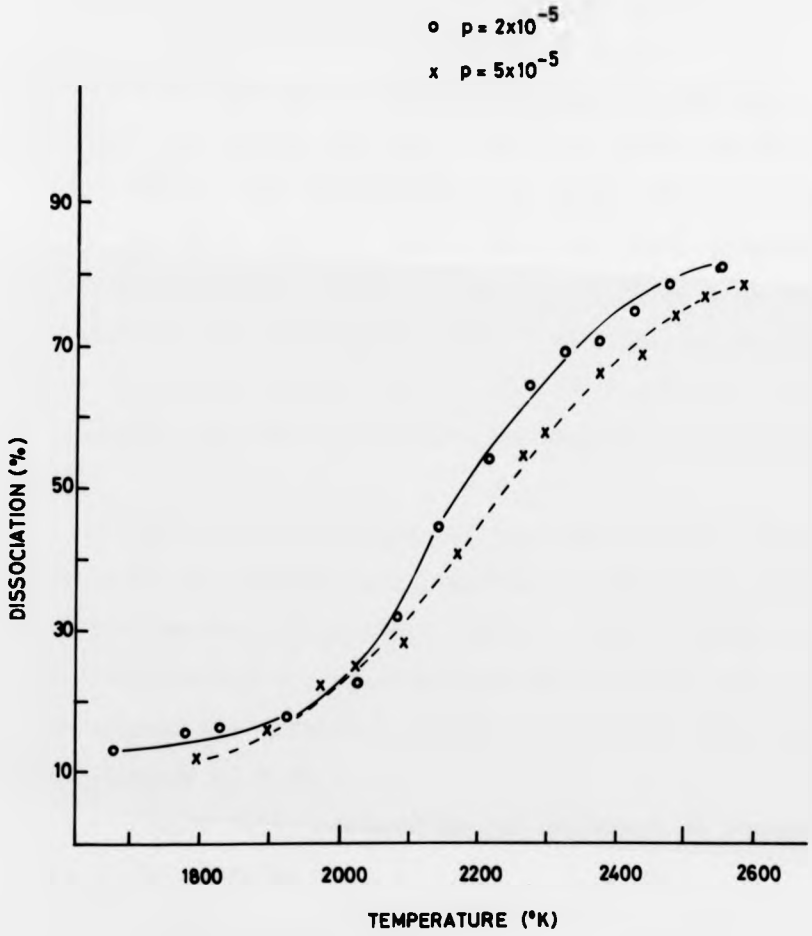

Fig.5.6.b Dissociation of hydrogen beam.

5.3 The Electron Monochromator

5.3.1 Introduction

Two main types of monochromators have been used in electron-atom scattering experiments, both of them use the deflection properties of electro-static fields. The hemispherical type with a deflection angle of 180^{o} was introduced by Simpson and Kuyatt (Simpson 1964; Kuyatt and Simpson 1967). The cylindrical type with a deflection angle of 127^{o} was first used by Clark (1954) and later improved by Marmet and Kerwin (1960). Many improvements have since been made for the cylindrical type. (Andrick and Ehrhardt 1966; Gibson and Dolder 1969). In this experiment, the cylindrical type was chosen since its design is mechanically simpler.

The deflection properties of the electrostatic field produced by two concentric cylindrical surfaces were first studies by Hughes and Rojanski (1930). Fig.5.7 shows the cylindrical deflector, the electrons are injected into the space between the cylinders through the entrance slit S_1 with an energy $E_o = eV_o$.

The radial field produced by the cylinders at potentials V_1 and V_2 is given by,

$$F = \frac{V_1 - V_2}{\log_e(R_2/R_1)} \quad \frac{1}{r}, \qquad (5.3.1)$$

where R_1 and R_2 are the radii of the inner and outer cylinders, respectively and $R_o = (R_1 + R_2)/2$ is the mean radius. An electron emerging perpendicularly from the entrance slit with energy $E_o = eV_o$ describes a circular path with radius R_o and is transmitted by the exit slit when the

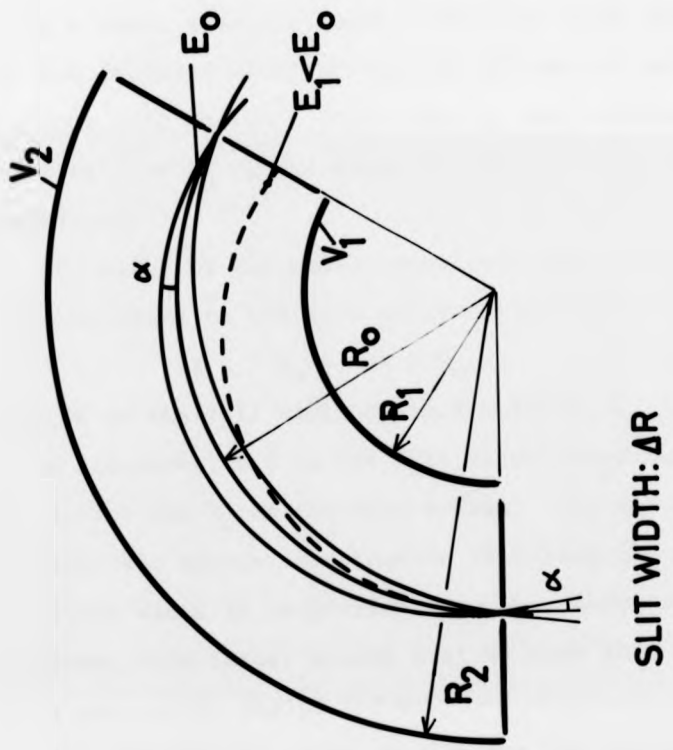

Fig.5.7 Cylindrical monochromator, schematic.

focussing condition,

$$2\,V_o = \frac{V_1 - V_2}{\log_e (R_2/R_1)} \qquad (5.3.2)$$

is fulfilled. The potential of the central orbit is chosen to be V_o, and V_1 and V_2 are symmetric with respect to V_o.

Hughes and Rojanski showed that all the electrons within a small aperture angle α emerging from the entrance slit are focussed after travelling through an angle of 127^o. Electrons with energies other than E_o are focussed at radii different from R_o in the plane of the exit slit and are not transmitted.

The width of the energy band selected by the monochromator is proportional to the slit width ΔR so that,

$$\Delta E / E_o = \Delta R / R_o, \qquad (5.3.3)$$

where ΔE is the full width at half maximum, E_o is the energy of the electrons, ΔR is the slit width (supposed equal for both slits) and R_o is the mean radius. For the ideal monochromator the energy distribution is triangular in shape.

Since width is proportional to the energy of the injected electrons, this latter energy must be kept low, and typical values are in the region 1-2 eV.

The theoretical value (5.3.3) for the energy width is not achieved in practice without further precautions. This is because aberrations, fringe effects and space charge have been neglected in the derivation of this formula. The effect of aberrations, which is the most serious, was taken into account in a second order theory by Delage and Carette (1971) and this leads to an energy width given by,

$$\Delta E / E_o = \Delta R / R_o + 4 \alpha^2 / 3 + \beta^2 \qquad (5.3.4)$$

where α is the half aperture angle of the beam emerging from the entrance slit in the plane of the drawing and β is the corresponding angle perpendicular to this plane. For an α of 10^o, the contribution of the second term is 0.04 i.e. 40 meV at an energy of 1 eV. It is thus important to limit the aperature angle of the beam to values smaller than 10 degrees. The contribution of the third term, determined by the slit height divided by the length of the central orbit, is smaller than 0.01 and can be neglected.

One of the experimental problems that had to be solved before the energy resolution of the cylindrical monochromator could be fully exploited was the elimination of those electrons that, on hitting the surface of the cylinders, are scattered back, so that some of them would be transmitted by the exit slit. Even if these electrons do not leave the monochromator, their space charge will distort the path of the other electrons. Marmet and Kerwin solved this problem by using high transparency grids instead of solid metal for the cylinders, so that the unwanted electrons would be transmitted and could be removed by a collector electrode placed behind the grids.

5.3.2 Mechanical Design

Fig. 5.8 shows the complete monochromator with injector, output lens and beam collector. The geometrical parameters listed in Table 5.1, closely followed those of Marmet and Kerwin, but in order to reduce fringe effects, the total height of the cylinders was increased to 50 mm.

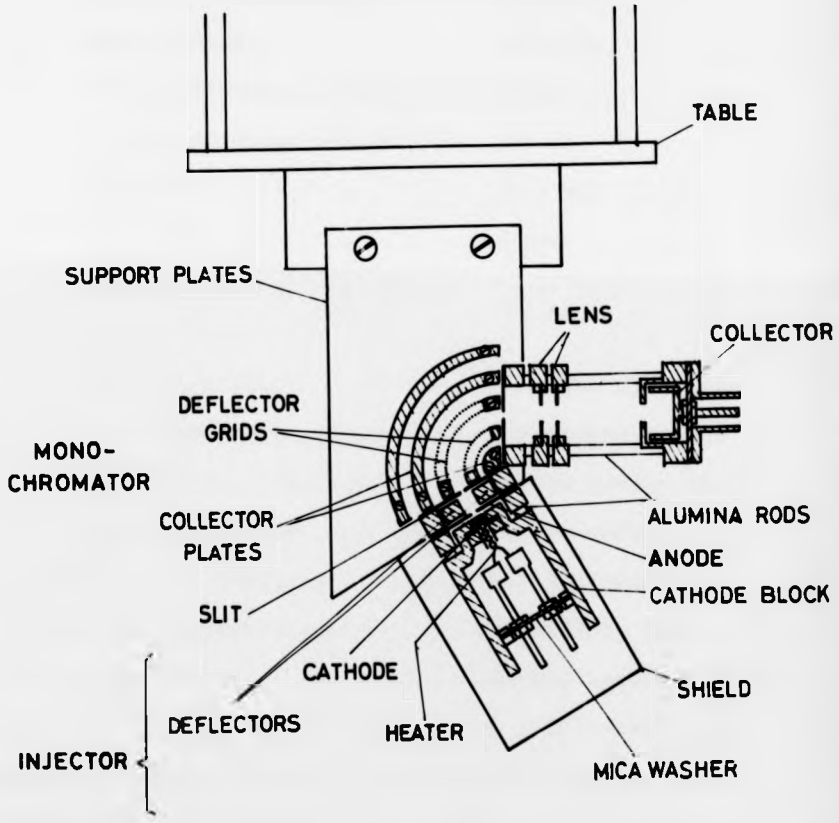

Fig.5.8. Electron monochromator

Table 5.1

Geometry of Monochromator

Radius of inner grid:	10 mm
Radius of outer grid:	15 mm
Mean radius:	12.5 mm
Radius of inner collector:	5 mm
Radius of outer collector:	20 mm
Slit width:	0.7 mm
Slit length:	5 mm
Total height of monochromator:	50 mm

The mode of operation is as follows. The electrons emitted by the thermionic cathode are accelerated by the anode to about 50 eV. The slit in the anode limits the aperture angle of the beam, and the electrons enter the monochromator at an energy of 1.5 eV after deceleration. The beam is then energy dispersed and focussed by the cylindrical deflectors. The energy selected beam emerging from the exit slit is accelerated to its final energy and focussed on to the collector by the aperture lens.

The aim of this design was to obtain a beam of electrons with an energy width of less than 100 meV and a total current of more than 10^{-8}A. For this reason rather broad slits of 0.7 mm width were used, and with an electron energy of 1.5 eV, the theoretical energy width according to (5.3.3) is 84 meV. The aperture angle of the beam can be approximated by the width of the anode slit divided by the distance from anode to slit. With a slit of 1 mm and a distance of 8 mm this leads to an

additional term in the energy width according to (5.3.4) of 20 meV, resulting in a total width of about 100 meV.

Copper was chosen as material for most of the monochromator, since it is non magnetic and easy to machine. However, all slits and apertures were made using molybdenum sheet with a thickness of 0.2 mm and the apertures and slits were spark eroded to close tolerances. They were then fitted as masks on to copper frames. The deflecting grids were made by winding thin tungsten wire 0.02 mm in diameter on to the cylindrical frames with a wire spacing of 0.3 mm. The transparency of the grids was thus greater than 90%. The two collectors were solid.

The injector is a simple diode stage which produces a narrow beam of electrons at about 50 eV. The cathode is mounted in a stainless steel block and held by a split ring which can be pressurized by a screw. An impregnated oxide cathode (Philips BP1A) with a diameter of 3 mm was used. The helical heater was held by two stainless steel legs, mounted on a mica washer and could easily be removed from the cathode block for replacement. The anode, with a slit opening of 1 mm x 6 mm, was also made of molybdenum on a stainless steel frame. It is important that all parts close to the cathode that become hot are made of molybdenum or stainless steel. Copper for instance poisons the cathode very quickly. The injector is aligned by four alumina rods with a diameter of 2.3 mm. In order to prevent the escape of electrons from the injector it was enclosed in a box made of tantalum sheet.

The output side consisted of a double aperture lens

with a diameter of 6 mm which accelerated the beam to its final energy and focussed it on to the beam collector, which was insulated from its housing by a mica washer. The output stage was aligned on four alumina rods which fitted into close tolerance holes in the electrodes, and the elements were held at the correct spacing by small screws which were tightened against the rods.

The monochromator was supported at the top and bottom of the cylinders by two PTFE plates which also served as an insulator between the electrodes.

The electrodes were positioned using accurately drilled holes in the plates, and fastened with small nonmagnetic screws. These plates, with their large area of insulating material, were a potential source of drifts and they were later replaced by stainless steel plates using alumina bushes as insulators.

5.3.3 Electrical Supplies and Field Cancellation

In scattering experiments with high energy resolution, electric and magnetic fields have to be reduced to small values. The collision region between the lens and the collector was at earth potential in order to avoid electric fields in or near the interaction region, which could destroy the metastables.

Constant voltage high stability supplies were used for all the electrodes except for the deflector grids. The grids were supplied by 9 volt batteries and the voltage was adjusted by Helipot high stability potentiometers. A constant current source was used for the cathode heater.

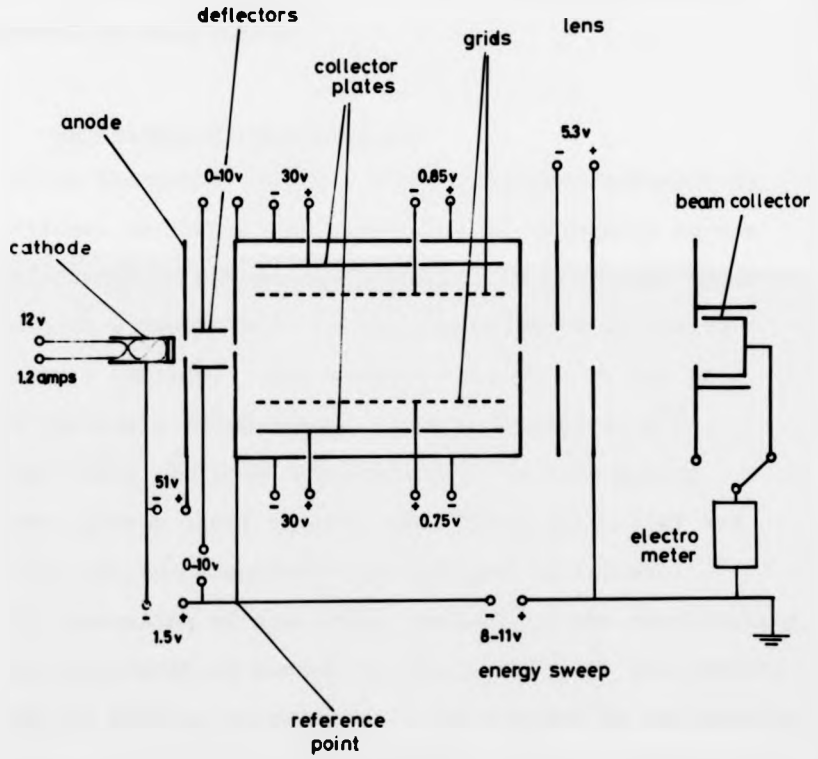

Fig.5.9. Monochromator, electrical supplies.

Fig.5.9 shows a schematic diagram with characteristic voltages.

The earth's magnetic field was reduced to less than 10 milligauss by a set of three pairs of Helmholtz coils, orthogonal to each other.

5.3.4 Operating Characteristics

Since the energy width ΔE of the monochromator is proportional to the energy itself, it is necessary to use slow electrons in the monochromator. In practice, space charge puts a lower limit to the energy since it limits the maximum current. The maximum current that can be passed through a fixed volume is proportional to $E^{3/2}$ (Simpson 1964) and thus decreases rapidly with energy. The lower energy limit in this experiment was 1.2 eV and normally, the monochromator was operated at 1.5 eV.

The focussing of the output current by the accelerating lens was monitored by measuring the currents to the Faraday cup and its housing separately. The current to the housing was small (about 20% of the collector current) and focussing conditions did not change with energy. There was, however, a small increase in the current as the energy was increased of 4% /volt which had to be taken into account when the measurements of the excitation function were made. The current as a function of energy was monitored and the count rates were corrected for the increase.

The diameter of the electron beam was smaller than that of the atom beam, ensuring that all the collector current had passed through the atom beam. Under these conditions,

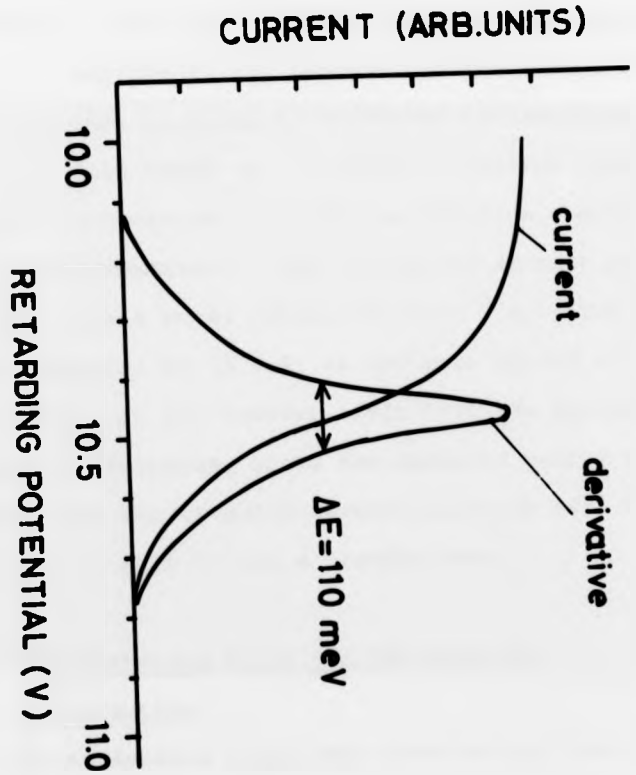

Fig.5.10 Energy distribution of electron beam.

small variations in the current density distribution across the atom beam do not influence the total excitation rate since they happen within a region of nearly constant atom density.

The electron energy distribution was determined by applying a retarding potential to the collector and measuring the current reaching the collector, as a function of the potential. The plot of the collector current against the potential represents the integral of the energy distribution, which was then obtained by graphical differentiation.

Fig. 5.10 shows the energy distribution resulting from the retardation curve for an electron energy of 1.5 eV in the monochromator. The full width at half maximum was 110 meV, with a total current of 7×10^{-9} A. The theoretical value according to (5.3.4) is 100 meV, giving a very good agreement. It is, however, felt that the agreement is somewhat fortuitous, since the measured energy distribution differs from the commonly assumed Gaussian with the same halfwidth in that it has a broader base.

5.4 The Quenching Field and the Detector

5.4.1 Introduction

The metastable atoms were detected by quenching in an electric field, where they emit a Lyman-alpha photon by decaying to the ground state via the 2p-state.

The mean lifetime T of the 2s-atoms in an electric field E is given by

$$T = (2780\ E^2)^{-1} \qquad (5.4.1)$$

where E is in V/cm and T is in sec (Bethe and Saltpeter 1957).

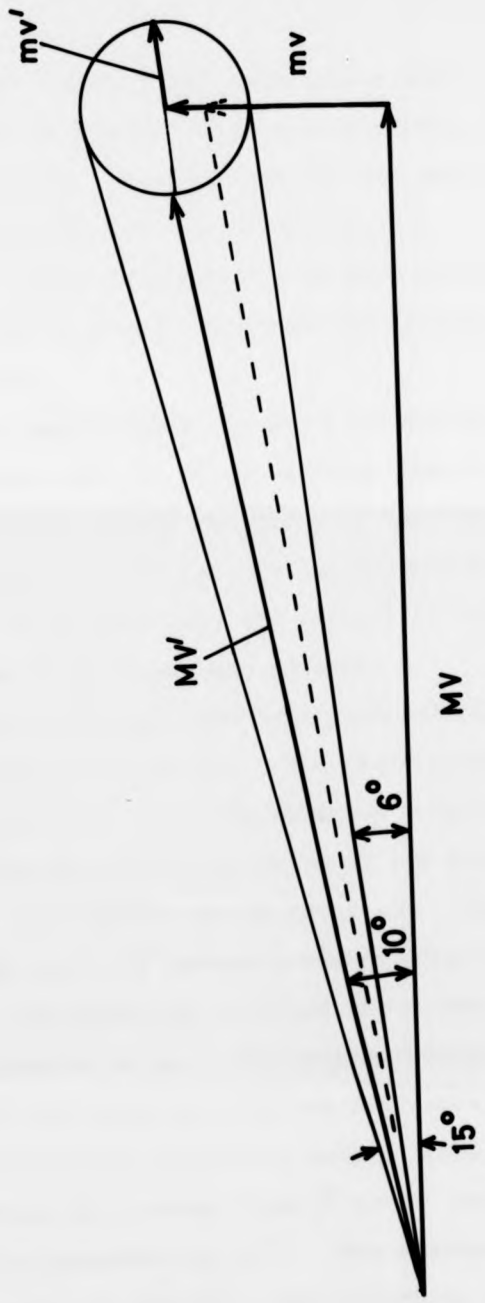

Fig.5.11. Momentum diagram for e - H collisions at 12 eV.

The mean decay length of the metastables with a velocity of 6×10^5 cm/sec in a field of 15 V/cm according to equation (5.4.1) is 1.2 cm. The requirements for well defined quenching conditions are the following:

1. The quench field should be well localised in order to prevent premature quenching of the 2s-atoms;
2. The quench field should be extensive enough to accept all the 2s-atoms which should all be quenched within the field of view of the detector. The recoil experienced by the 2s-atoms when they are excited by the electrons has to be taken into account.

A uniform field produced by a parallel plate condenser with guard plates was chosen. The field strength was 15 V/cm. Fig. 5.11 shows the momentum diagram for an inelastic collision with excitation of the H-atom to the n=2 state at an electron energy of 12 eV. The H-atom has a velocity of 6.3×10^5 cm/sec corresponding to a temperature of $2500^{\circ}K$. Its momentum is MV and the momentum of the impinging electron is mv. The corresponding momenta for the atom and the electron after the collision at MV' and mv'. The horizontal deflecting angle, lying in the plane of the drawing, has a range from 6° to 15° and the mean deflection is approximately 10°. The maximum vertical deflection angle is only 5°. The situation at threshold (10.2 eV) is indicated by the broken line, and the deflection angle in this case is 9°. The main point here is that the variation in the distribution in this energy range is small.

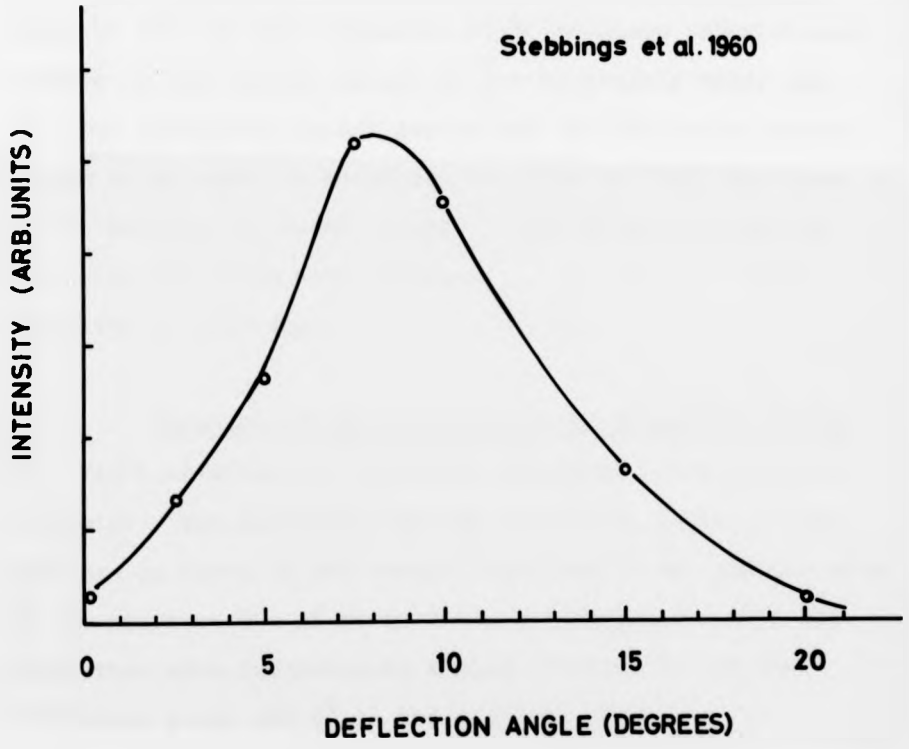

Fig.5.12. Angular distribution of H(2s) atoms (Stebbings et al. 1960).

If this variation were large, the metastable beam would change its position in space and this would have to be taken into account. Stebbings, Fite, Brackmann and Hummer (1960) made measurements of the angular distribution of the metastables as a function of energy shown in Fig.5.12. At 12 eV the mean deflection angle is 9^{o} and the maximum angle is 20^{o}, in good agreement with the above calculations. Because of the angular spread of the metastable beam, the distance between the quench region and the excitation region should be as small as possible, in order to limit the size of the beam in the quench field. Loss of metastables by collision quenching with residual gas molecules is also minimized in this way.

5.4.2 Geometry of Quenching Field and Mechanical Design

Fig.5.13 shows the detection geometry, which is drawn to scale. The distance from the excitation region to the aperture in front of the quench field was 70 mm, and the size of the aperture was 35 mm x 20 mm, big enough to admit all atoms that were deflected by angles of up to 15^{o} in the horizontal plane and 8^{o} in the vertical plane.

Since the decay length of the metastables in the electric field of 15 V/cm is about 1.5 cm, the detector has to view the first 3-4 cms of the field. A vertical section of the quench field and the detector is shown in Fig.5.14.

A system of two pairs of plates was used to produce the field, with the outer plates acting as guard plates to reduce the stray field. Each pair of plates is biased alternately and this arrangement has the effect of pulling

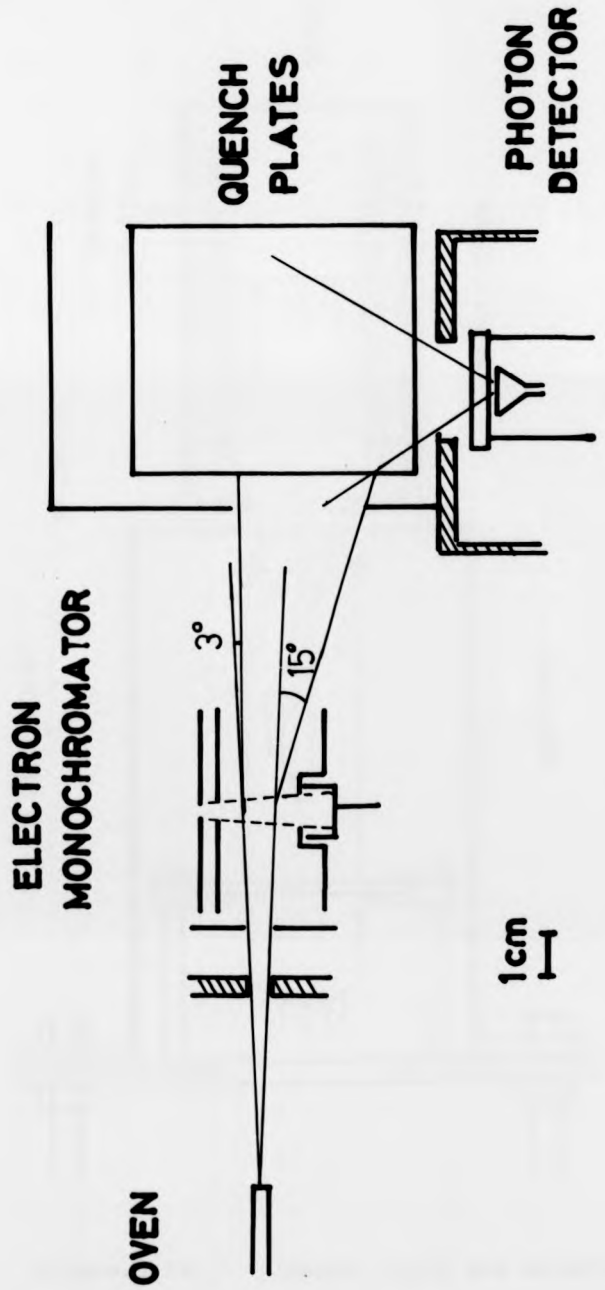

Fig.5.13 Geometry of detection

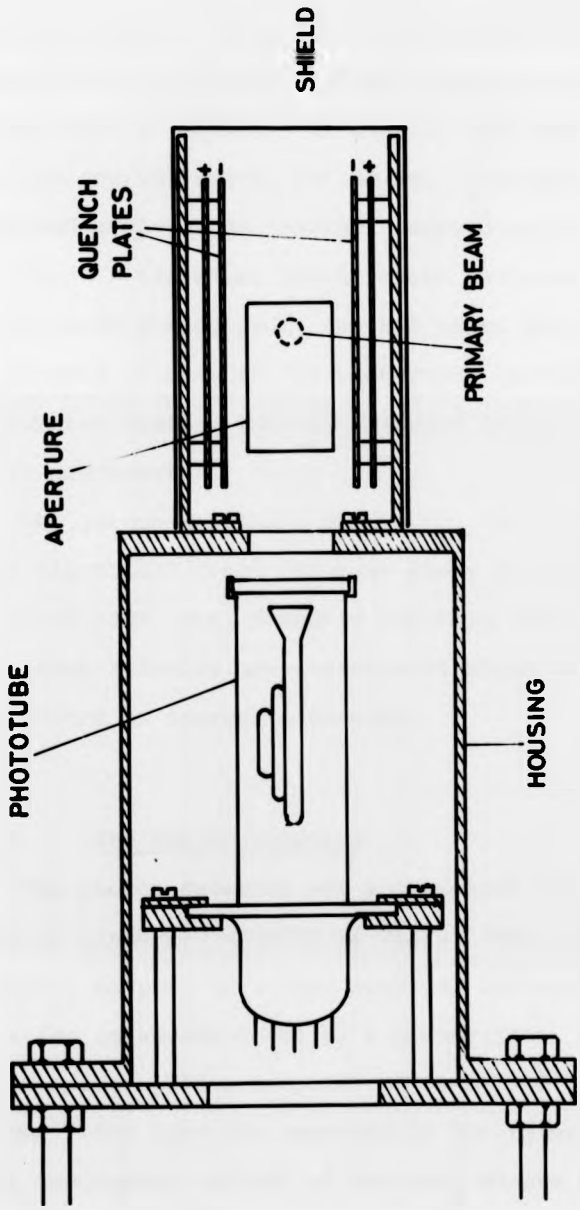

Figure.5.14. Quench field and detector.

the field lines back and reducing the stray field. (Kauppila, Ott and Fite 1970). The size of the plates was 70 mm x 70 mm, and each pair was insulated by alumina spacers with a thickness of 3 mm. The central spacing, i.e. the quench region, was 30 mm. The plate pairs were supported by L-shaped brackets screwed on to the detector housing. A stainless steel shield enclosed the quench region, with the aperture for the beam, and this shield effectively eliminated the background photons from the interaction region, and the residual stray fields of the quench condenser.

The quench radiation emitted by the metastable atoms in an electrical field has been shown to have a polarization of -30% (Ott, Kauppila and Fite 1970) but this does not affect relative measurements of cross sections since this effect is energy independent.

5.4.3 The Photon Detector

The photon detector was a phototube with a magnesium-fluoride window. (Bendix BX 762). The cathode, which is funnel shaped, is coated with CsI and electron multiplication is accomplished by a channeltron. The tube is very compact, with a diameter of 32 mm and a length of 120 mm. The tube was operated in the pulse mode. The short wavelength cut-off of the MgF_2 window is at 1140 Å, and on the long wavelength side, the quantum efficiency

of the CsI photocathode drops to 0.008% at 2000 Å, compared with the value of 8% at 1216 Å, the wavelength of the Lyman-alpha line. This means that the tube is effectively "solar-blind", which is very important since the hydrogen furnace is an intense source of visible light and the expected signal was only in the order of a few counts per second. The dark count rate of the tube was about 0.2 counts/sec. The channeltron electron multiplier, when operated in the saturated mode, has the advantage of a high gain of 10^8 combined with a narrow Gaussian pulse height distribution making it easy to discriminate against noise.

The voltage divider for the channeltron and the coupling capacitor were mounted directly on the tube in order to keep electrical connections as short as possible minimizing the risks of interference. The phototube was housed in a stainless steel cylinder, as shown in Fig.5.14 and this shielded the HV connections, the resistor network and the capacitor.

This photon detector can also be used for the measurement of the excitation functions in krypton and xenon, since at 1500 Å, the quantum efficiency is still above 5%. The efficiency drops to half its peak value (8% at 1250 Å) at a wavelength of 1600 Å.

5.5 Modifications for the Heavy Rare Gases

In the case of the heavy rare gases krypton and xenon, the excitation function of states with optically allowed transitions to the ground state were measured and a different arrangement of the detector and monochromator was used, with the detector viewing the interaction region. The phototube was mounted at right angles to the electron and atom beams on the support table as shown in Fig.5.15. All the components of the table were made of nonmagnetic stainless steel, and the table was held by four rods fixed on the flange which also contained all the feedthroughs, so that the table could be easily withdrawn from the tank.

The electron monochromator was unchanged except for the replacement of the PTFE support plates by stainless steel plates. The screws holding the electrodes were insulated by alumina bushes which were diamond cut from alumina tubes. As a result of this improvement, the stability of the output current was increased since the total area of the insulators had been drastically reduced by the change.

Adjustment of the phototube was accomplished by sliding its housing in the collar, while the monochromator support bracket could be moved along two slots cut into the table. The atom beam crossed the electron beam at right angles.

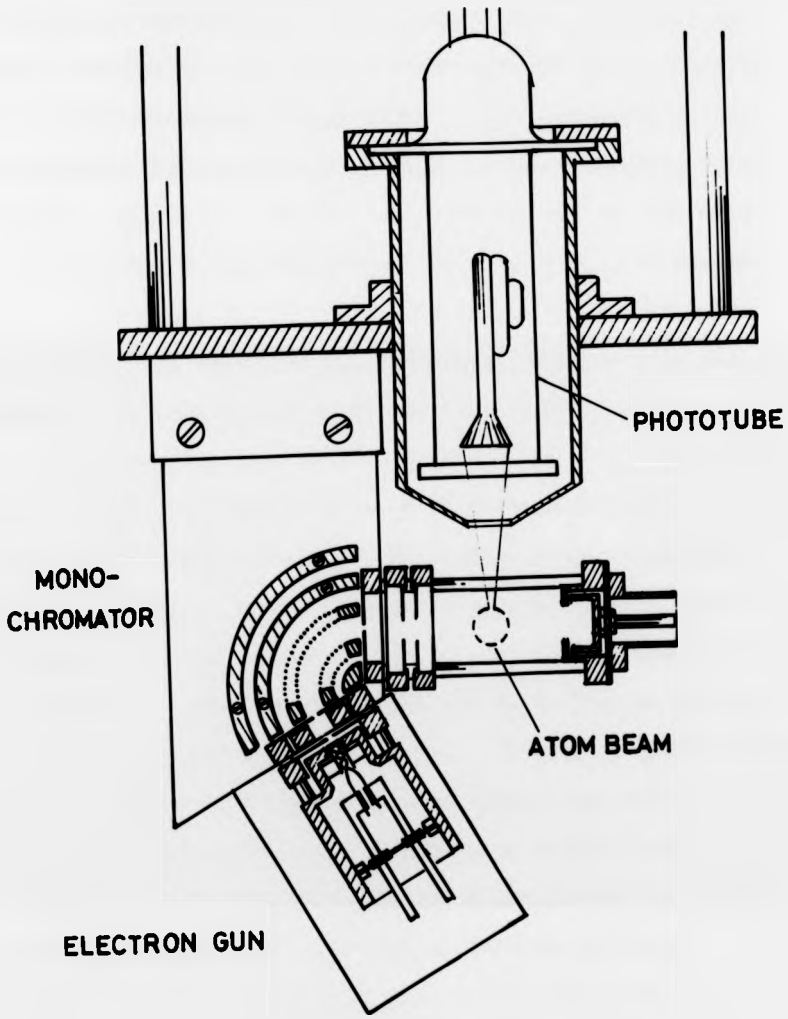

Fig.5.15 Detector arrangement for excitation measurements in krypton and xenon.

The experiments were carried out on a small one-chamber apparatus which had been used as a test apparatus for the electron monochromator. The chamber was evacuated by a mercury diffusion pump with a speed of 150 l/sec baffled by a liquid nitrogen cooled trap. For accurate energy calibration, the krypton experiments were repeated on the hydrogen apparatus. Using a mixture of helium and krypton, the energy scale was calibrated by observing the helium elastic resonance at 19.35 eV and the krypton excitation function. The electron spectrometer described in the thesis by V. Raible was used for this purpose.

Since krypton and xenon are monoatomic at room temperature, the source does not have to be heated and can be brought much closer to the interaction region than the hydrogen source. A cylindrical stainless steel tube with a diameter of 2 mm and a length of 130 mm was used as the beam source. The distance from the beam source to the interaction region was only 15 mm. Research graded gases in pyrex flasks were sealed to the apparatus and the gas flow to the source was controlled by a needle valve.

The gas flow was measured in a simple way by closing the butterfly valve to the diffusion pump and measuring the pressure rise in the chamber due to the gas flow as a function of time. The throughput $\Delta Q / \Delta t$ is given by

$$\frac{\Delta Q}{\Delta t} = \frac{\Delta p \; V}{\Delta t}, \qquad (5.5.1)$$

where Δp is the pressure rise in the time interval Δt and V is the volume of the chamber. This is then multiplied by 3.54×10^{19} to give the flow N in molec/sec. At a

The experiments were carried out on a small one-chamber apparatus which had been used as a test apparatus for the electron monochromator. The chamber was evacuated by a mercury diffusion pump with a speed of 150 l/sec baffled by a liquid nitrogen cooled trap. For accurate energy calibration, the krypton experiments were repeated on the hydrogen apparatus. Using a mixture of helium and krypton, the energy scale was calibrated by observing the helium elastic resonance at 19.35 eV and the krypton excitation function. The electron spectrometer described in the thesis by V. Raible was used for this purpose.

Since krypton and xenon are monoatomic at room temperature, the source does not have to be heated and can be brought much closer to the interaction region than the hydrogen source. A cylindrical stainless steel tube with a diameter of 2 mm and a length of 130 mm was used as the beam source. The distance from the beam source to the interaction region was only 15 mm. Research graded gases in pyrex flasks were sealed to the apparatus and the gas flow to the source was controlled by a needle valve.

The gas flow was measured in a simple way by closing the butterfly valve to the diffusion pump and measuring the pressure rise in the chamber due to the gas flow as a function of time. The throughput $\Delta Q / \Delta t$ is given by

$$\frac{\Delta Q}{\Delta t} = \frac{\Delta p \; V}{\Delta t} , \qquad (5.5.1)$$

where Δp is the pressure rise in the time interval Δt and V is the volume of the chamber. This is then multiplied by 3.54×10^{19} to give the flow N in molec/sec. At a

background pressure of 2×10^{-5} Torr the gas flow was 8×10^{15} molec/sec. The gas density n(O) at the end of the tube can be approximated by,

$$n(O) = \frac{N}{c \pi a^2} \quad . \qquad (5.2.5)$$

With a = 0.1 cm and $c = 2.5 \times 10^4$ cm/sec the density at the end of the tube is $n(O) = 10^{13}$ at/cm^3. The corresponding mean free path λ is

$$\lambda = (n q \sqrt{2})^{-1} \quad . \qquad (5.2.6)$$

With the above value for n and $q = 9 \pi \times 10^{-16}$ cm^2 the mean free path is 25 cm, so that at least part of the tube seems to be in molecular flow conditions. However, the gas density increases very rapidly towards the high pressure end of the tube and the mean free path decreases accordingly. Zugenmaier (1960) gives an expression for the density increase along the tube as a function of the distance z from the tube end as a linear relation,

$$n(z) = g + fz, \text{ with } f = \frac{3N}{2 \pi c a^3} \text{ and } g = \frac{2N}{\pi c a^2} \qquad (5.5.2)$$

These expressions show that molecular flow conditions certainly do not prevail along the whole length of the tube. However, intermediate flow conditions with $\lambda > a$ are fulfilled at least for the first 5 cm and the formulae of paragraph 5.2.1 apply. Thus,

$$J(\theta = 0) = \frac{3^{\frac{1}{2}} c^{\frac{1}{2}} a^{\frac{1}{2}} N^{\frac{1}{2}}}{8 \pi^{\frac{1}{2}} 2^{\frac{1}{4}} \sigma} \quad , \qquad (5.2.3)$$

and with a = 0.1 cm, $N = 8 \times 10^{15}$ at/sec, $\sigma = 3 \times 10^{-8}$ cm, the beam intensity in the forward direction is $J(O) = 10^{16}$ at/sterad sec. The beam flux density at a distance of 1.5 cm is $I = 5 \times 10^{15}$ at/cm^2 sec. The corresponding beam number density is $n = 2 \times 10^{11}$ at/cm^3.

In section 7.2.1 the dependence of the signal on the beam intensity will be investigated.

6. Electronics and Data Acquisition

6.1 General Description

The electronics of the experiment are shown in Fig.6.1. The detector pulses were fed into an emitter follower in order to match the output impedance of the multiplier to that of the cable. The integral discriminator following the amplifier was set to about 5% of the mean pulse height which suppresses all noise without affecting the signal. The normalized pulses from the discriminator were then fed into a scaler. At higher count rates a ratemeter was used for continuous monitoring. For the cross section measurements, the multichannel analyser was used. The contents of the scaler and the analyser could be read out on a typewriter.

6.2 Multichannel Analyser and Energy Scanning

In order to make full use of the time available for the actual integration of counts, automatic data acquisition is necessary. The time available for measurement was usually limited by breakdowns, mainly of the hydrogen source. Because of the low signal count rates for hydrogen, long integrating times were expected and this raises the problem of how to overcome drifts in the experimental parameters.

One answer to this problem is to use rapid scanning of the energy range in a time which is short compared to the drift times in the intensity of the atom beam and electron beam. A multichannel analyser was used in its multiscaling mode in such a way that the electron energy was synchronized with the channel number. The energy

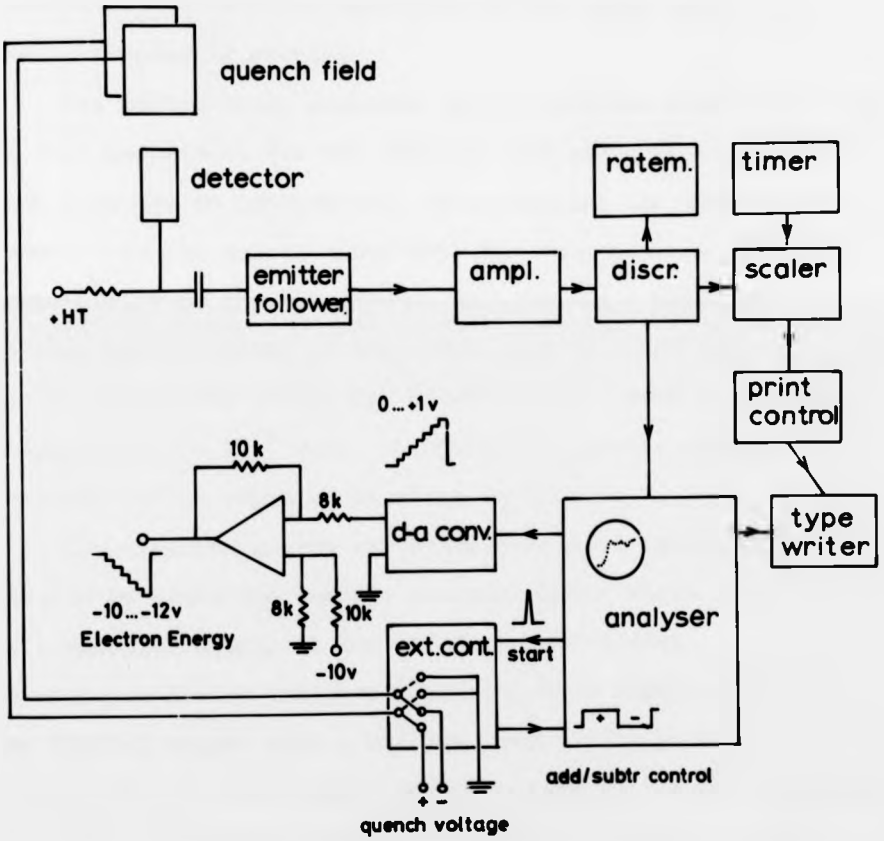

Fig.6.1. Electronics .

range could be scanned in a few seconds (about 0.1 sec per channel) a large number of times until the signal-to-noise ratio was high enough. The contents of each channel are a measure of the relative magnitude of the cross section at the corresponding energy.

The multichannel analyser (Intertechnique DIDAC 800) used in this experiment has 800 channels and any number smaller than this can be preselected, thus defining the scanning range. In the multiscaling mode the channels are addressed sequentially by a clock module, and the dwell time per channel can be preset to any value from 10^{-5} sec upwards, during which time counts are accumulated. Dead time beteen channels is 5×10^{-6} sec. A cycle of a preset number of channels can be repeated as often as desired.

The electron energy was synchronized to the channel advance by using the running channel number which is available as a parallel output in BCD coded decimal format. A digital-to-analogue device (Advance Electronics DA 120B) converted the digital output into a voltage ramp with a swing from 0 to 8 volts for the full number of 800 channels, and an operational amplifier was used to invert and amplify the output of the converter, since a negative voltage was required to control the energy of the electrons. The step height of the voltage staircase was chosen to be 25 meV, so that 100 channels were needed to cover the range from 10.0 to 12.2 eV. Fig.6.1 shows the details of the circuit.

Subtraction of the background counts was also done automatically using the external control facilities of the multichannel analyser. The add and subtract modes of the analyser can be controlled by a DC voltage. This voltage

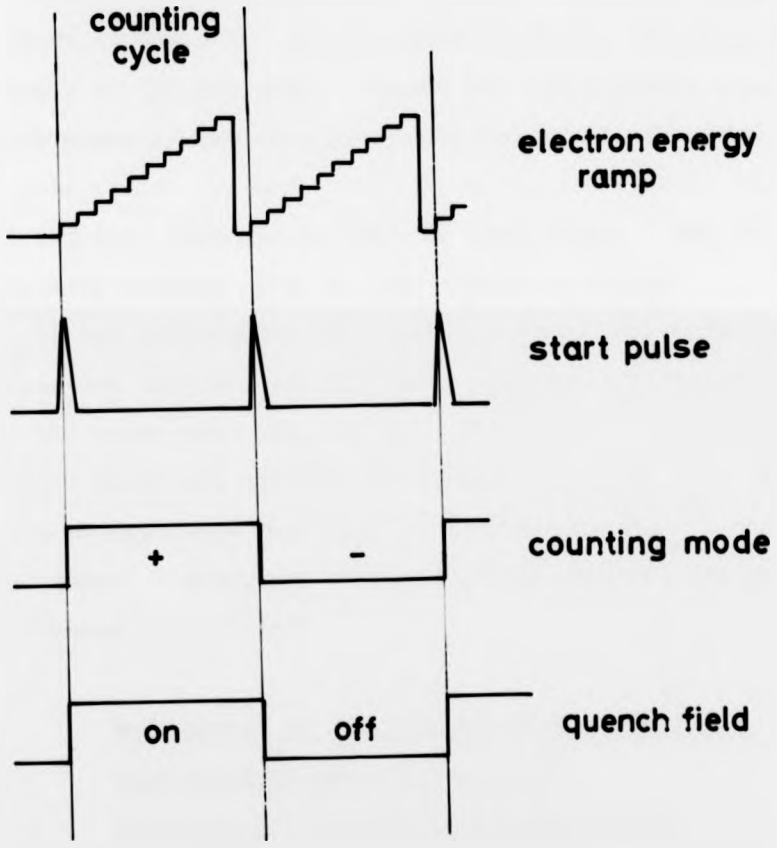

Fig.6.2. Counting sequence .

was provided by a bistable circuit, triggered by a pulse at the completion of one cycle, which in turn, switches the quench field by activating a relay. The time sequence is shown in Fig.6.2. At the start of a run, the analyser is reset to the add mode. During the first cycle, signal + background is accumulated (quench field on), and during the next cycle, the background is subtracted (quench field off) and this sequence is repeated many times. The run is eventually stopped after an even number of cycles.

In the experiments with the rare gases, the background subtraction facility was no longer needed. The background i.e. the count rate with the beam off, which only amounted to about 5% of the signal, was almost a constant over the entire energy range and could be substracted after a separate measurement. Also, the step width when scanning the energy was reduced to 12.5 meV.

7. Measurement of the Excitation Cross Sections

7.1 Excitation of the 2s-state in H

7.1.1 Alignment of Apparatus and Signal Tests

The atom beam cross section in the excitation region is given by the size of the collimating aperture in the oven chamber wall, as shown in Fig.5.13. The electron monochromator and the quench field collimator were aligned with respect to the beam aperture using a telescope. Alignment of the oven was achieved by linear movement of the oven flange and smaller corrections were made using the setting screws at the oven flange.

The position of maximum signal coincided with the

position of optical alignment, with a typical oven temperature of 2600°C and an oven chamber pressure of 7×10^{-5} Torr.

The 2s-signal is given by the difference of the count rates with the quench field on and off, thus,

$$S = C_{on} - C_{off} = (S + B) - B \quad . \qquad (7.1.1)$$

The background B comes from two sources. Firstly, excitation of atomic and molecular hydrogen by the electron beam yielding ultraviolet photons, mainly Lyman-alpha photons from the decay of the 2p state. Secondly, and predominantly, excitation of hydrogen that takes place in the oven itself by electron emission from the oven heater. These two sources of background were minimized by the shield in front of the quench region and typical values were 0.2/sec for the first (with an electron current of 10^{-8} A) and 1/sec for the second. Typical signal count rates were 4/sec.

The signal was then tested for spurious effects. One such spurious signal can arise from stray electrons which enter the quench field and are accelerated when the field is switched on. This can lead a false signal due to excitation processes in the background gas. This effect eliminated by the shielding of the quench region as described in Section 5.4.2. There was no "signal" below the n=2 threshold at 10.2 eV.

Since about 20% of the beam and most of the background gas consists of molecular hydrogen, the possibility of spurious H_2 effects has to be taken into account. However, with the oven at room temperature, that is with a pure H_2 beam, no "signal" was detected in the energy range of interest from 10 to 13 eV. At energies above 14.7 eV one would

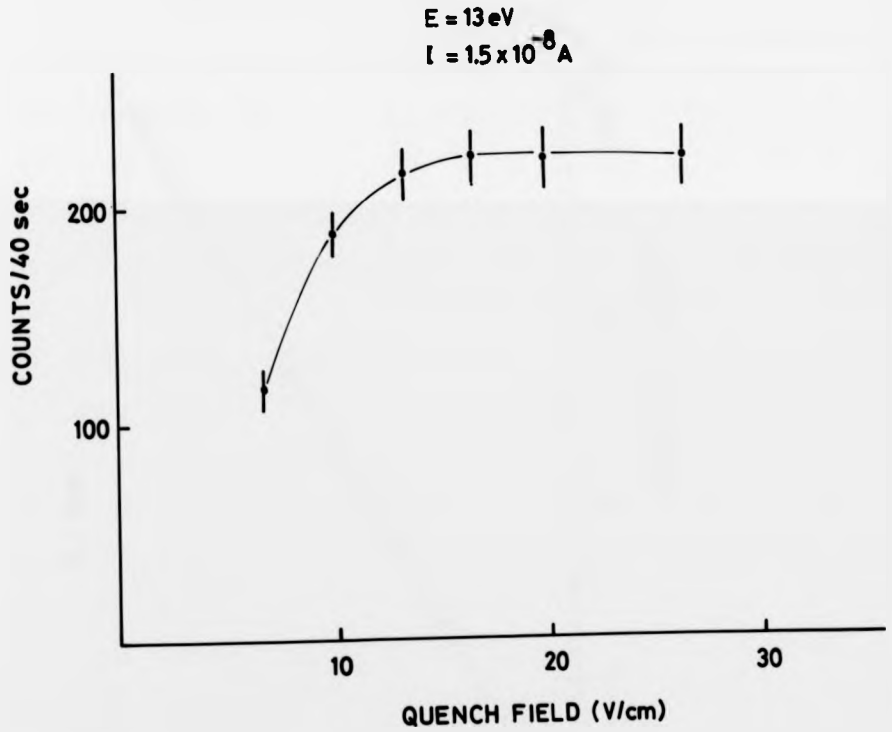

Fig.7.1. Dependence of 2s-signal on the quenching field.

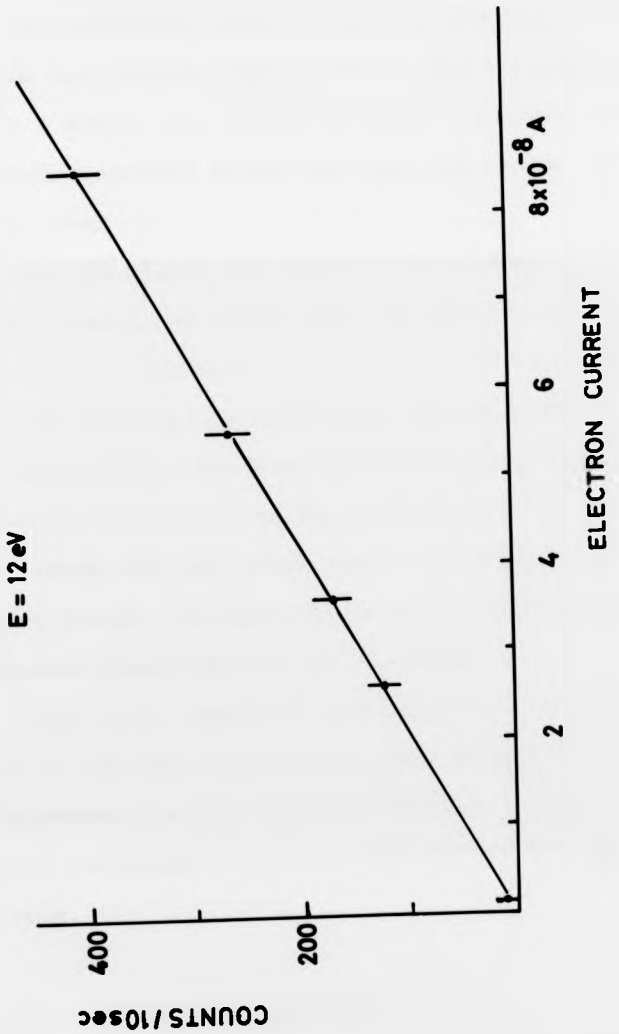

Fig.7.2. Dependence of 2s-signal on the electron current.

expect 2s-atoms produced by dissociative excitation of H_2 since the dissociation energy of the molecule is 4.5 eV.

The fact that the 2s atoms, which carry the information, can only be formed from atomic hydrogen, is the main reason for the relatively good signal to background ratio of about 3:1 in the present experiment. After accumulating for about 4 hours, the signal-to-noise ratio was about 10:1. The main limiting factor was the low signal count rate of about 4/sec.

The 2s signal was measured as a function of the quench field strength to check that all the metastables were indeed quenched by the field. Saturation of the signal at 15 V/cm, as shown in Fig.7.1, indicated that all the metastables were quenched within the field of view of the counter, and that premature quenching can be neglected. If such an effect were important one would expect the signal to decrease at higher fields, because higher stray fields would cause premature quenching of the 2s atoms.

The total number of excitations is given by equation (3.1.3) and the signal count rate should therefore be proportional to the electron current. Fig.7.2 shows the linear relationship between the signal and the electron current.

7.1.2 Cross Section Measurements

In order to eliminate the influence of drifts in beam intensity, the energy range was scanned quickly with typical counting times per channel of 200 m sec, so that with 100 channels for the whole energy range (25 meV/ch) each cycle

takes 20 sec to complete. The measurements of the degree of dissociation described in Section 5.2.3 showed that the time constants for drifts in the beam intensity much larger than this.

The oven chamber pressure, the excitation chamber pressure and the electron current were monitored in order to detect changes in the experimental conditions. Since the electron current as a function of energy did not remain absolutely constant but showed a slight increase of about 4%/volt, the data points had to be corrected for this.

Although the electron monochromator had been stabilized for 6-10 hours before the start of the experimental runs, a small energy drift of the electron beam was still a possibility, since the monochromator could not be baked at temperatures of above 100°C. Such an energy drift would be noticed as a decrease in the apparent energy resolution and the steep rise in the cross section at threshold provides a sensitive test for this. A decrease in the slope of the threshold rise could indeed be observed in runs lasting 8 hours or more, and in order to minimize this effect, the integration time for each run was limited to 3-4 hours. Fig.7.3 shows two of these runs. The signal to noise ratio in each case is about 12:1.

According to equation (7.1.1) the signal is given by,

$$S = C_{on} - C_{off} = (S + B) - B \ .$$

The standard deviation of the signal ΔS is then given by,

$$\Delta S = \sqrt{S + 2\,B} \ , \qquad (7.1.2)$$

and the signal-to-noise ratio by,

$$S/\Delta S = S \,/\, \sqrt{S + 2\,B} \ , \qquad (7.1.3)$$

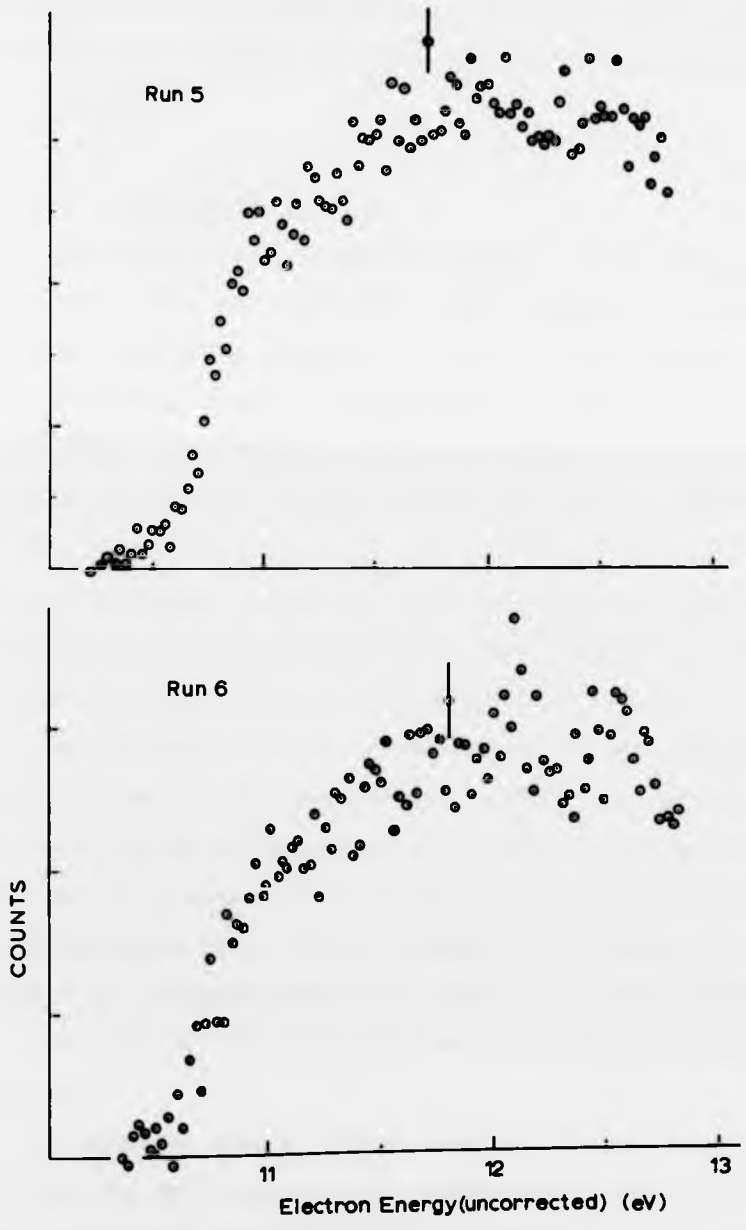

Fig.7.3 Single measurements of 1s - 2s excitation function. The vertical scale is in arbitrary units.

Measurements of the background, which was a smooth curve rising slowly with energy, were made at the beginning and end of each run.

7.1.3 Evaluation of Data

Eight final runs similar to those in Fig.7.3 were made. The results of these runs were added, thereby increasing the signal-to-noise ratio by a factor of three compared with the single runs. Energy shifts between the runs had to be taken into account, they were always less than two channels or 50 meV. Between the group of the first five and the last three runs there was a shift of 250 meV which can be attributed to the fact that the apparatus had to be opened to atmosphere because of an oven breakdown and the electron monochromator had to be stabilized again.

The procedure for the normalization of the energy scale was as follows. The steep onset of the cross section at threshold can be approximated by a linear function and the intersection of this line with the energy axis was used as the normalizing point for the energy. The measured value of the n = 2 threshold was 10.80 and 11.10 eV for the first and second group, compared with the spectroscopic value of 10.20 eV.

In order to obtain absolute values for the cross section, the measurements were normalized to the theoretical results that are available in the threshold region. (Taylor and Burke 1967), (Burke, Ormonde and Whitaker 1967) (Geltman and Burke 1970), all shown in Fig.4.2. The latter probably give the best absolute values in the intermediate region

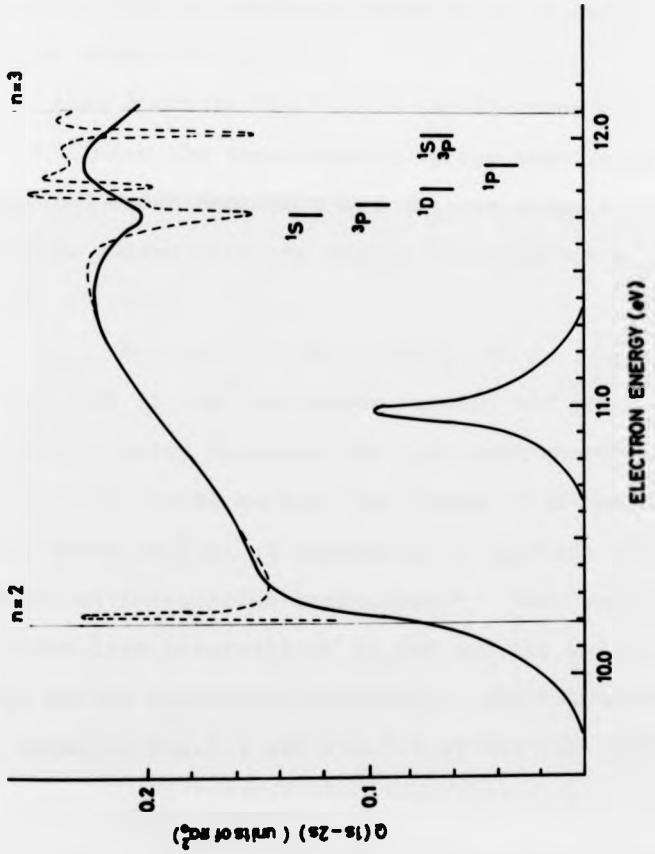

Fig.7.4 1s - 2s excitation cross section in H.

Broken curve: theory, renormalized.
Full curve: theory, folded with experimental energy distribution, inserted at the bottom.

between 10.5 and 11.0 eV. In order to obtain one continuous theoretical curve both the 3-state + correlation approximation and the 6-state approximation were renormalized to the best results of Geltman and Burke in the intermediate region, where they overlap. The main effect of this is that the cross section at energies above 11 eV is reduced by about 8%, as shown in Fig. 7.4.

Also shown in Fig.7.4 is the electron energy distribution, which limits the experimental energy resolution. The measured cross section σ exp (E_o) is given by the true cross section folded with the energy distribution of the electron beam, so that,

$$\sigma_{exp}\ (E_o) = \int_{-\infty}^{+\infty} \sigma\ (E)\ j\ (E-E_o)\ dE \ /\ \int_{-\infty}^{+\infty} j\ (E-E_o)\ dE, \quad (7.1.4)$$

where $\sigma(E)$ is the true cross section and $j(E-E_o)$ is the electron energy distribution with mean energy E_o. The theoretical cross section was folded with the energy distribution shown in Fig.7.4 according to equation (7.1.4) using numerical integration techniques.* Both curves were subdivided into intervals of 10 meV and the calculations were done on the university computer. The folded cross section is shown in Fig.7.4 and Fig.7.5 as the full curve.

7.1.4 Final Results

Fig. 7.5 shows the final results for the excitation cross section of the 2s-state in atomic hydrogen. These results were normalized to theory in the region between 10.6 and 10.8 eV, where the cross section is smooth and structureless. This is also the region where the best

---

* The limits of integration where chosen as $E_o + 4\Delta E$ and $E_o - 4\Delta E$, beyond which $j\ (E-E_o)$ is practically zero.

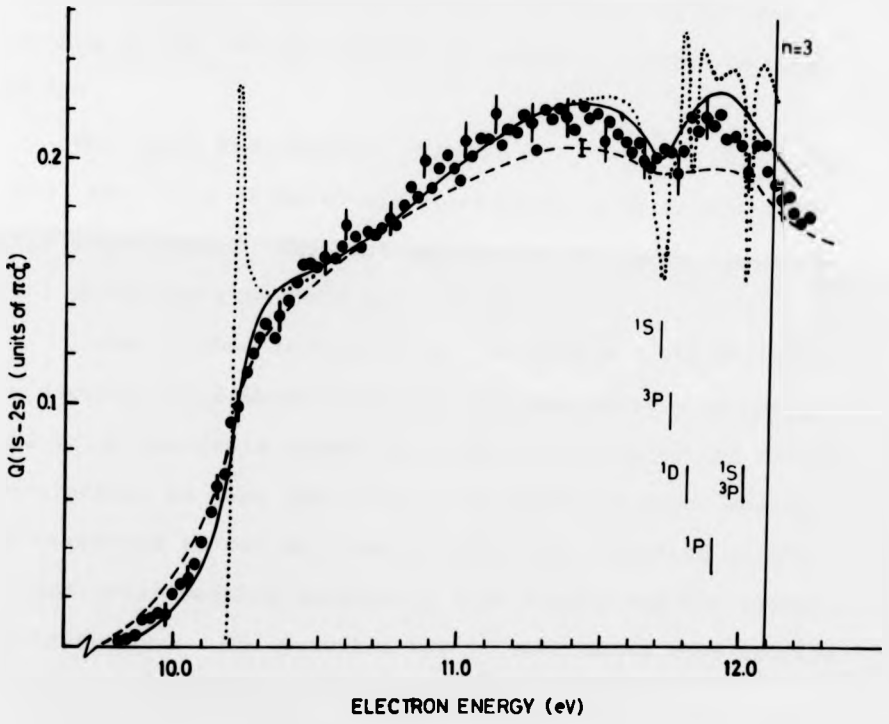

Fig.7.5 1s - 2s excitation cross section in H, normalized to theory. Closed circles: this work, error bars show one standard deviation; dotted curve: theory; solid curve: folded theory; dashed curve: experiment by Oed. The position of the resonances predicted by Burke et al (1967) is also shown.

results of Geltman and Burke are available.

The main feature of the results is the resonance structure at 11.75 ± 0.05 eV, which is a superposition of the ^1S and ^3P resonances at 11.72 and 11.75 eV predicted by theory. Each of these has a width of about 40 meV but because of the strong overlap the resulting width is near 80 meV.

The other resonances, ^1D at 11.81, ^1P at 11.90, ^1S at 12.03 and ^3P at 12.04 eV are too narrow to be resolved in this experiment. The same applies to the shape resonance just above the threshold at 10.22 eV.

There is some indication of the energy drift discussed in section 7.1.2 which could not be completely eliminated and which manifests itself in a deterioration of the energy resolution, in that the rise of the measured cross section at threshold is not as steep as expected according to the folded cross section calculated from theory and the energy distribution. One possible way of overcoming this problem would be to make the monochromator fully bakeable.

The agreement between this experiment and the folded theory is good, but there is a small but systematic deviation of the experimental points toward smaller values at energies above 11.3 eV. There is also good agreement with the experiment of Oed (1971) which was published during the course of the present experiment. Oed's results were normalized to the present ones at 10.80 eV. Oed specifies an energy resolution of 150 meV. At the higher energies, Oed's results are lower than the present ones by about 5%. Both experiments thus indicate that the cross

section curve is flatter in the region from 10.6 eV to the n=3 threshold than the six-state close coupling approximation.

7.2 Measurement of the Excitation Function of the $4p^5$ 5s Stakes in Krypton and of the $5p^5$ 6s States in Xenon

7.2.1 Experimental Procedure and Tests

The dependence of the signal on the electron beam current and the target gas density for Krypton and Xenon is shown in Figs.7.6 and 7.7. The more interesting of these is the dependence on the gas pressure. The target gas density in the beam could not be measured directly, and the gas pressure in the chamber is a measure of the total gas flow rather than the intensity of the beam itself. From the estimates of Section 5.5, indicating that there is intermediate flow with a square root dependence of the beam intensity on the total flow, a square root dependence of the signal on the chamber pressure would be expected and the measured results are shown in Fig.7.7, which on a log-log scale, show straight lines with slopes of 0.43 and 0.60, in good agreement with the predictions.

At higher pressures the atom beam spreads and the background gas density becomes greater than the beam density, since the former rises linearly with the gas flow compared with the slower rise of the latter. This leads to a linear rise of the signal. This change occurred at pressures of about 8×10^{-5} Torr, and the measurements were carried out at lower values. The signal is thus proportional to the beam density and trapping of the resonance photons can be neglected. As a further test, a series of excitation

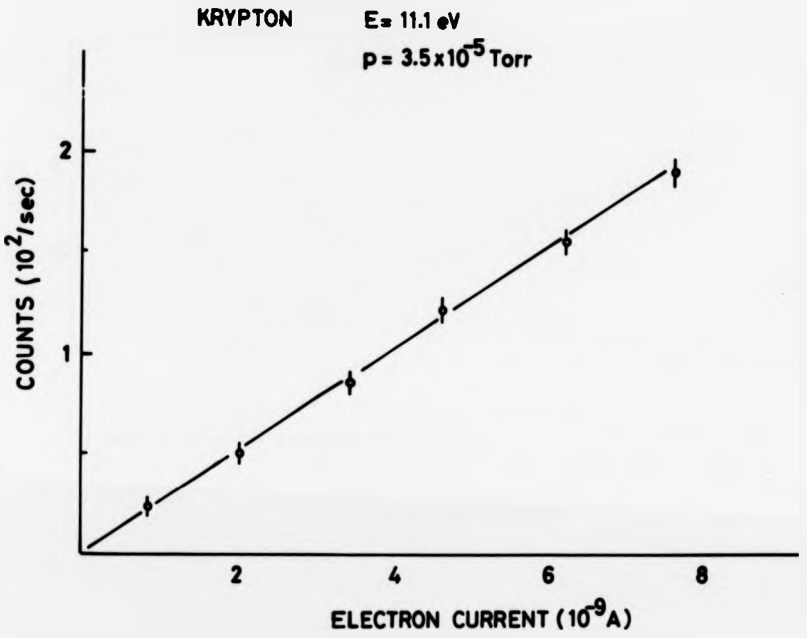

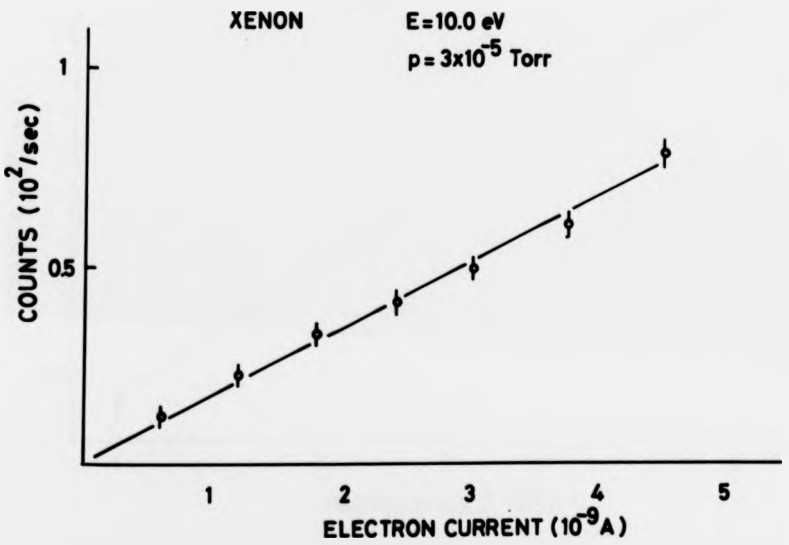

Fig.7.6 Dependence of the photon count rate on the electron current for krypton and xenon.

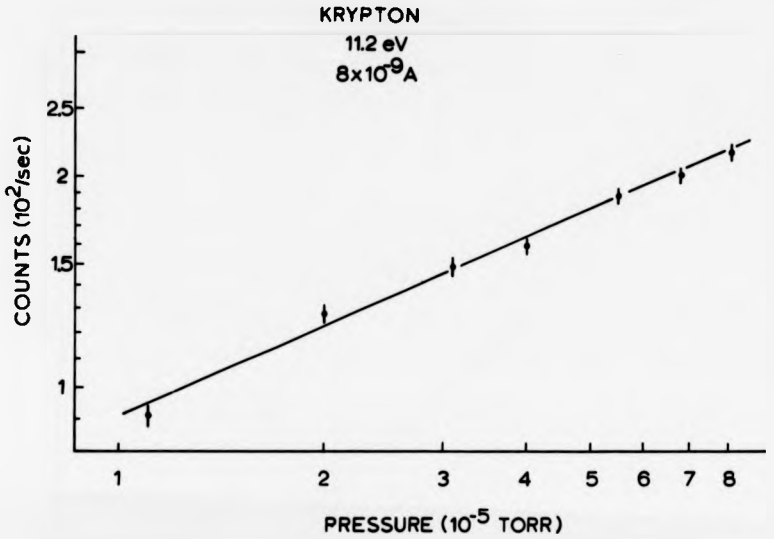

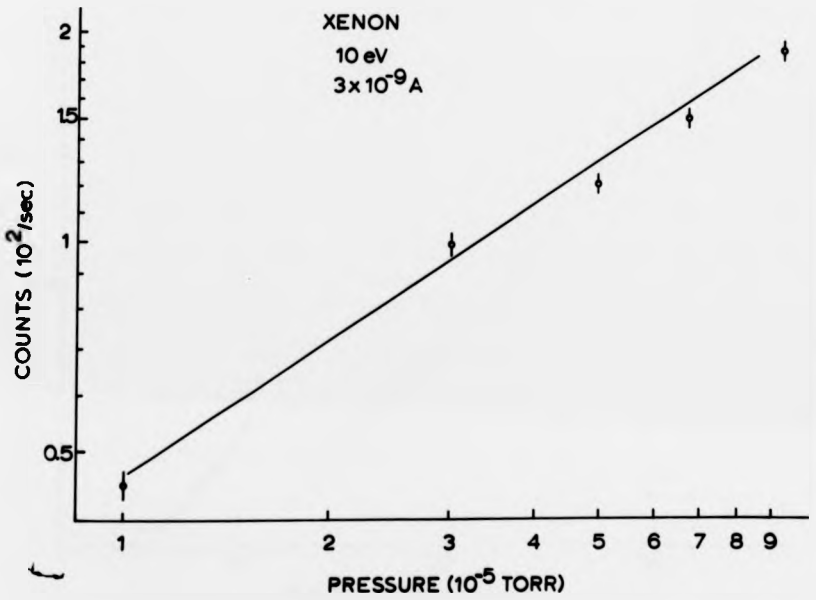

Figure 7.7 Dependence of photon count rate on the total pressure for krypton and xenon.

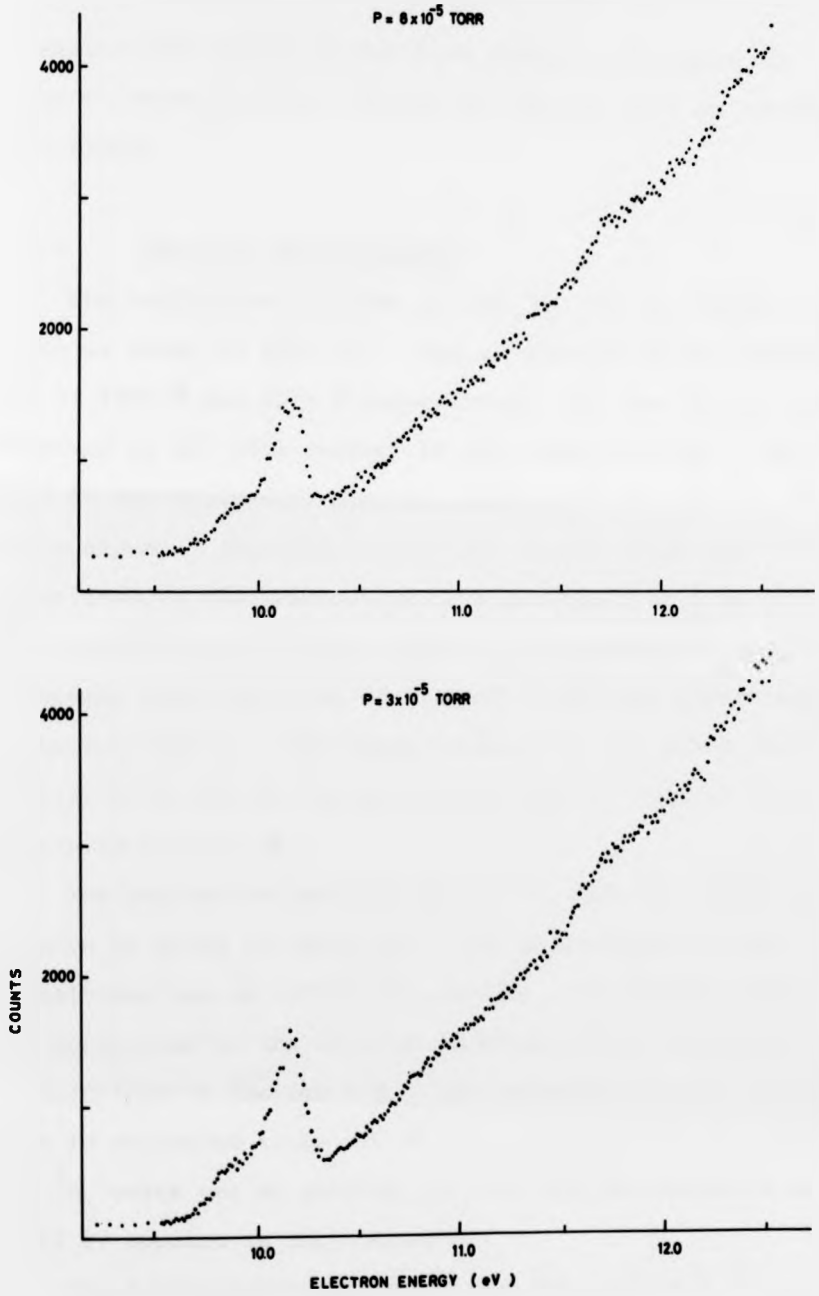

Fig.7.8 Excitation of krypton at different total pressures.

functions were taken at different chamber pressures for krypton, shown in Fig. 7.8 and the results show no pressure dependence.

7.2.2 Results and Discussion

The excitation function of the $^3P_1$ and $^1P_1$ levels in xenon is shown in Fig.7.9. The wavelength of the transitions are at 1469 Å and 1294 Å respectively, and the photons were observed at 90° with respect to the electron beam. Below 9.57 eV the excitation function represents that of the $^3P_1$ state alone. (See Fig.3.3). The energy scale was normalized to the xenon excitation threshold at 8.44 eV. The peak at 9.25 eV of the present measurements is in good agreement with the value of 9.20 eV of Elston, Lawton and Pichanick (1973). The steep increase of the cross section at 9.60 eV is due to the opening of the $^1P_1$ channel at its threshold of 9.57 eV.

The excitation function of the $^3P_1$ and $^1P_1$ states in krypton is shown in Fig.7.10. The wavelengths of the transitions are at 1235 Å and 1164 Å. The energy scale was normalized to the 19.35 eV elastic helium resonance, as described in Section 5.5. The accuracy of this calibration is estimated to be ± 0.05 eV. Below 10.64 eV, only the $^3P_1$ state can be excited, and the strong resonance at 10.15 eV appears in this channel.

The lowest resonance states are the $(4p^5\ 5s^2)\ ^2P_{3/2,\ 1/2}$ states of Kr^-, and the splitting between these is closely approximated by the fine structure splitting of the $(4p^5)$ $^2P_{3/2,\ 1/2}$ states of Kr^+, since the closed s^2 subshell does

functions were taken at different chamber pressures for krypton, shown in Fig. 7.8 and the results show no pressure dependence.

7.2.2 Results and Discussion

The excitation function of the $^3P_1$ and $^1P_1$ levels in xenon is shown in Fig.7.9. The wavelength of the transitions are at 1469 Å and 1294 Å respectively, and the photons were observed at 90^o with respect to the electron beam. Below 9.57 eV the excitation function represents that of the $^3P_1$ state alone. (See Fig.3.3). The energy scale was normalized to the xenon excitation threshold at 8.44 eV. The peak at 9.25 eV of the present measurements is in good agreement with the value of 9.20 eV of Elston, Lawton and Pichanick (1973). The steep increase of the cross section at 9.60 eV is due to the opening of the $^1P_1$ channel at its threshold of 9.57 eV.

The excitation function of the $^3P_1$ and $^1P_1$ states in krypton is shown in Fig.7.10. The wavelengths of the transitions are at 1235 Å and 1164 Å. The energy scale was normalized to the 19.35 eV elastic helium resonance, as described in Section 5.5. The accuracy of this calibration is estimated to be $\pm$ 0.05 eV. Below 10.64 eV, only the $^3P_1$ state can be excited, and the strong resonance at 10.15 eV appears in this channel.

The lowest resonance states are the $(4p^5\ 5s^2)\ ^2P_{3/2,\ 1/2}$ states of Kr^-, and the splitting between these is closely approximated by the fine structure splitting of the $(4p^5)$ $^2P_{3/2,\ 1/2}$ states of Kr^+, since the closed s^2 subshell does

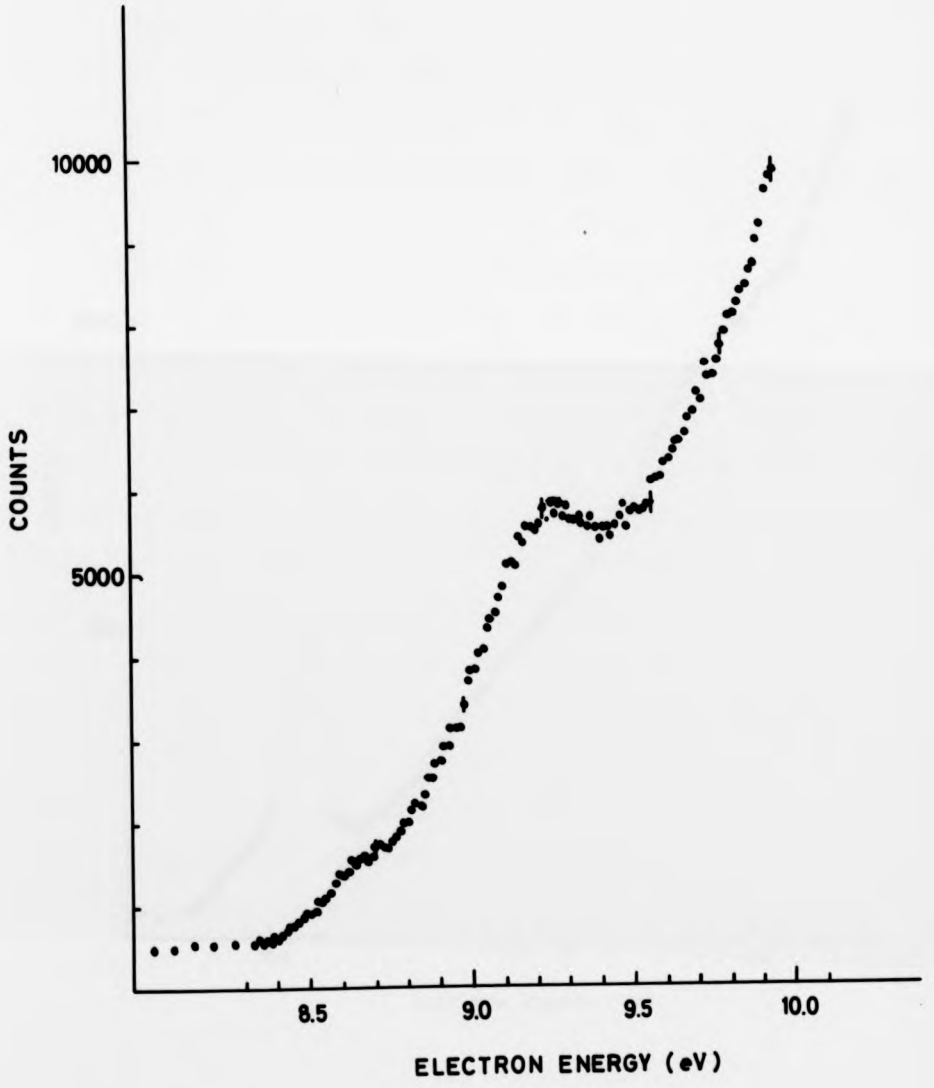

Fig.7.9 Excitation cross section (in arbitrary units) of the $5p^5 6s\ ^3P_1$ and $^1P_1$ states in xenon. Error bars indicate one standard deviation.

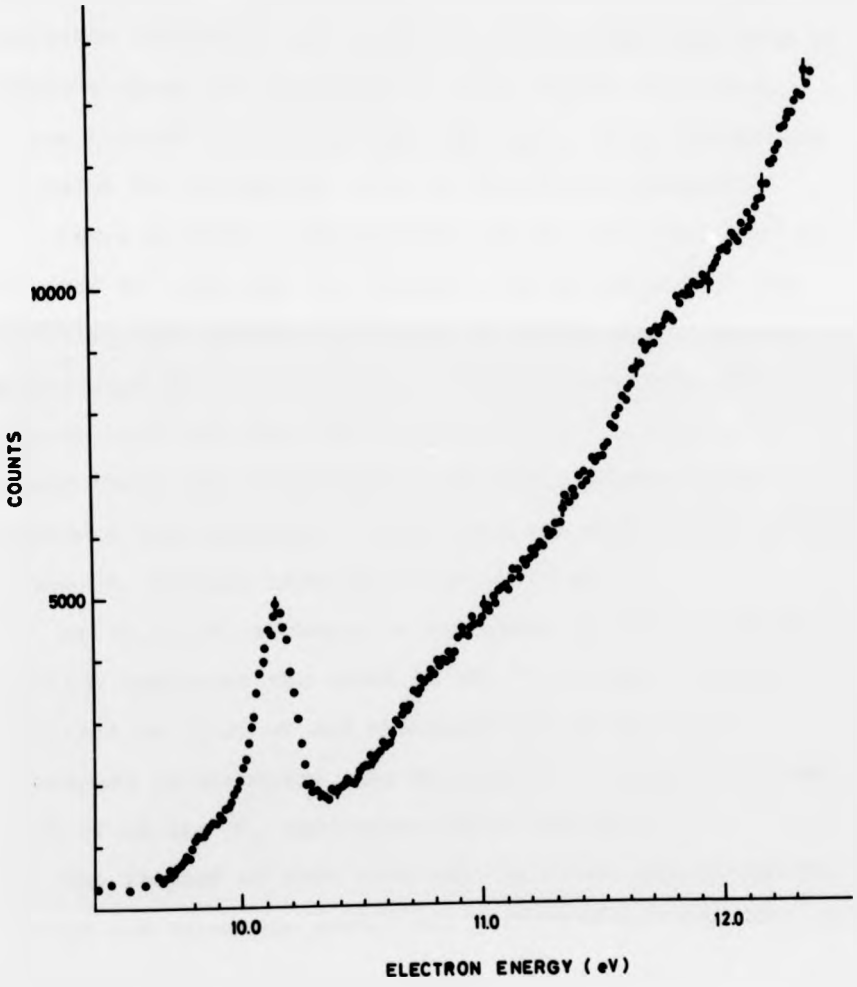

Fig.7.10 Excitation cross section (in arbitrary units) of the $4p^5 5s\ ^3P_1$ and $^1P_1$ states in krypton. Error bars indicate one standard deviation.

not influence the fine structure greatly. In krypton the splitting is 0.66 eV and in xenon it rises to 1.30 eV. Since the lower $^2P_{3/2}$ resonance lies about 0.5 eV below the inelastic threshold, the upper $^2P_{1/2}$ resonance must take up position above the threshold in both krypton and xenon. In the lighter rare gases neon and argon, these resonances lie below the threshold, i.e. in the elastic channel.

There is thus a strong decay of the resonance $(4p^5\ 5s^2)$ $^2P_{1/2}$ of Kr^- into the $^3P_1$ channel, and by comparison its effect in the elastic scattering is rather small (Kuyatt, Simpson and Mielczarek 1965). Similar results to the present ones have been obtained by Swanson, Cooper and Kuyatt (1973) who investigated inelastic scattering of electrons from krypton. They found the same strong resonance in the $^3P_1$ channel locating it at 10.14 eV.

At 10.65 eV, a change in the slope of the excitation function indicates the onset of the $^1P_1$ state. Discontinuities at 11.35 eV and the broad dip at 12.15 eV correspond to structure seen by Swanson et al at 11.29 and 12.15 eV in the $^1P_1$ excitation cross section.

The results of this work and the other experiments on krypton and xenon are summarized in Tables 7.1 and 7.2 below.

Table 7.1

Resonances in Krypton

Classification	Transmission (Kuyatt et al 1965)	Metastable Production (Pichanick & Simpson 1968)	Transmission (Sanche & Schulz 1972)	Scattering (Elston et al 1973)	This Work
$4\ p^5_{1/2}\ 5s^2$	10.10 eV		10.16 eV	10.14 eV	10.15 eV
		10.63	10.66	10.67	10.65
		11.20	11.29	11.29	11.35
		11.48	11.40	11.42	
		11.70	11.67	11.66	
		12.04	12.10	12.04	12.15

Table 7.2

Resonances in Xenon

Classifi-	Transmission (Kuyatt et al 1965)	Transmission (Sanche & Schulz 1972)	Optical Excitation (Elston et al 1973)	This Work
		8.48 eV	8.54 eV	8.70 eV
$5p^5_{1/2}\ 6s^2$	9.33 eV	9.11-9.26	9.20	9.25
	9.45	9.65	9.70	

The strong resonance in krypton at 10.15 eV is a convenient energy calibration point, since it is easy to observe and does not require the use of an electron analyser, as in the case of the 19.35 eV elastic resonance in helium.

7.3 Conclusions and Suggestions for Further Work

The atomic beam apparatus described here has been shown to be a very versatile piece of equipment, suitable for making measurements of elastic, inelastic and excitation cross section measurements. The considerable problems associated with atomic hydrogen beams have not been completely solved, and it would be well worth carrying out the following improvements, designed to overcome the problems of the low signal-to-noise ratio and the stability of the apparatus over long periods of time.

1. The hydrogen beam density should be increased, and this could be done by the use of a multi-channel source. Electron bombardment, which is a more effective method of heating, would then become necessary.
2. The molecular background gas in the excitation chamber should be reduced. Such a reduction is very important in such applications as elastic and inelastic electron scattering measurements. The reduction of the background pressure could be achieved by introducing a buffer chamber between the oven chamber and the excitation chamber which would cut down the gas load of the excitation chamber.

3. The long term energy stability of the electron monochromator should be improved. Since the problem seems to be associated with a drift of contact potentials due to surface contamination, the best method to overcome this problem is to bake the monochromator regularly and to keep it at a temperature of about 200°C during the measurements. An increase in the resolution could then be achieved since drifts would be eliminated, and longer integration times could be used, improving the signal-to-noise ratio.

Points 2 and 3 also apply to measurements on other gases, such as the heavy rare gases. Some of the excitation processes could be investigated with greater energy resolution. Angular distribution of scattered electrons and of emitted photons could also be studies using this apparatus.

REFERENCES

D. ANDRICK and H. EHRHARDT, Z. Phys 192, 99 (1966)

G. BECKER, Z. Angew. Phys. 13, 59 (1961)

H. BETHE and E. E. SALPETER, in Handbuch der Physik, ed. by S. Flügge, (Berlin 1957) Vol. 35, p.373

R. T. BRACKMANN, W. L. FITE, R. H. NEYNABER, Phys. Rev. 112, 1137 (1958)

G. BREIT and E. WIGNER, Phys. Rev. 51, 593 (1937)

P. G. BURKE and H. M. SCHEY, Phys. Rev. 126, 147 (1962)

P. G. BURKE, Proc. Phys. Soc. 82, 443 (1963)

P. G. BURKE, S. ORMONDE and W. WHITAKER, Proc. Phys. Soc. Lond. 92, 319 (1967)

P. G. BURKE, Advances in Atomic and Molecular Physics, 4, 173 (1968)

G. E. CHAMBERLAIN and H. G. M. HEIDEMAN, Phys. Rev. Lett. 15, 337 (1965)

E. M. CLARKE, Can. J. Phys. 32, 764 (1954)

P. CLAUSING, Z. Phys. 66, 471 (1930)

D. M. COX and S. J. SMITH, in Abstracts of Papers of the VIIth International Conference on the Physics of Electronic and Atomic Collisions, Amsterdam 1971

Y. DELAGE and J. D. CARETTE, Can. J. Phys. 49, 2118 (1971)

S. B. ELSTON, S. A. LAWTON and F. M. J. PICHANICK, Abstracts of Papers of the VIIIth ICPEAC, Beograd 1973, Vol. I, p.480, Institute of Physics, Beograd 1973

W. L. FITE and R. T. BRACKMANN, Phys. Rev. 112, 1141 (1958)

W. L. FITE, R. F. STEBBINGS and R. T. BRACKMANN, Phys. Rev. 116, 363 (1959)

W. L. FITE in Atomic and Molecular Processes, Ed. by B. R. Bates, Academic Press, New York and London (1962)

P. S. GANAS and A. E. S. GREEN, Phys. Rev. A4, 182 (1971)

S. GELTMAN and P. G. BURKE, J. Phys. B.3, 1062 (1970)

J. R. GIBSON and K. T. DOLDER, J. Phys. B. Atom. Molec. Phys. 2, 741 (1969)

J. A. GIORDMAINE and T. C. WANG, J. Appl. Phys. 31, 463 (1960)

D. W. O. HEDDLE and R. G. W. KEESING, Advances in Atomic and Molecular Physics, 4, 267 (1968)

D. HILS, H. KLEINPOPPEN and H. KOSCHMIEDER, Proc. Phys. Soc. 89, 35 (1966)

A. L. HUGHES and V. ROJANSKI, Phys. Rev. 34, 284 (1929)

W. E. KAUPPILA, W. R. OTT and W. L. FITE, Phys. Rev. A1, 1099 (1970)

E. KISKER, Z. Physik 256, 121 (1972)

C. E. KUYATT, J. A. SIMPSON and J. E. MIELCZARCK, Phys. Rev. 138, A 385 (1965)

C. E. KUYATT and J. A. SIMPSON, Rev. Scient. Just. 38, 103 (1967)

W. E. LAMB and R. C. RETHERFORD, Phys. Rev. 79, 549 (1950)

W. E. LAMB and R. C. RETHERFORD, Phys. Rev. 81, 222 (1951)

W. LICHTEN and S. SCHULTZ, Phys. Rev. 116, 1132 (1959)

J. H. MACEK and P. G. BURKE, Proc. Phys. Soc. Lond. 92, 351 (1967)

P. MARMET and L. KERWIN, Can. J. Phys. 38, 787 (1960)

H. S. W. MASSEY and E. H. S. BURHOP, Electronic and Ionic Impact Phenomena, Oxford, Clarendon Press, 1969

J. W. McGOWAN, J. F. WILLIAMS and E. K. CURLEY, Phys. Rev. 180, 132 (1969)

B. L. MOISEIWITSCH and S. J. SMITH, Rev. Mod. Phys. 40, 238 (1968)

A. OED, Phys. Lett. 34A, 435 (1971)

W. R. OTT, W. E. KAUPPILA and W. L. FITE, Phys. Rev. A1, 1089 (1970)

F. M. J. PICHANICK and J. A. SIMPSON, Phys. Rev. 168, 64 (1968)

V. RAIBLE, Thesis, University of Stirling, 1974

N. F. RAMSEY, Molecular Beams (Oxford 1956) p.363

D. ROY and J. D. CARETTE, J. Appl. Phys. 42, 3601 (1971)

J. A. SIMPSON, Rev. Scient. Instr. 35, 1698 (1964)

L. SANCHE and G. J. SCHULZ, Phys. Rev. A5, 1672 (1972)

T. SAWADA, J. E. PURCELL and A. E. S. GREEN, Phys. Rev. A4, 193 (1971)

G. J. SCHULZ, Phys. Rev. Lett. 10, 104 (1963)

G. J. SCHULZ, Phys. Rev. Lett. 13, 583 (1964)

K. SMITH, P. R. McEACHRAN and P. R. FRASER, Phys. Rev. 125, 553 (1962)

K. SMITH, Reports on Progress in Physics, 29, 373 (1966)

R. F. STEBBINGS, W. L. FITE, D. G. HUMMER and R. T. BRACKMANN, Phys. Rev. 119, 1939, (1960)

G. SUNSHINE, B. B. AUBREY and B. BEDERSON, Phys. Rev. 154, 1 (1967)

N. SWANSON, J. W. COOPER and C. E. KUYATT, Phys. Rev. A8, 1825 (1973)

A. J. TAYLOR and P. G. BURKE, Proc. Phys. Soc. London, 92, 336 (1967)

J. F. WILLIAMS, J. Phys. B. Atom. Molec. Phys. 7, L56 (1974)

P. ZUGENMAIER, Z. Angew. Phys. 20, 184 (1966)

Attention is drawn to the fact that the copyright of this thesis rests with its author.

This copy of the thesis has been supplied on condition that anyone who consults it is understood to recognise that its copyright rests with its author and that no quotation from the thesis and no information derived from it may be published without the author's prior written consent.